Taylor & Francis
Taylor & Francis Group

Science and Technology of Advanced Materials: Methods

ISSN: (Print) (Online) Journal homepage: www.tandfonline.com/journals/tstm20

First-principles thermodynamic modeling for the Al-Nb-Ni ternary system

Arkapol Saengdeejing, Ryoji Sahara & Yoshiaki Toda

To cite this article: Arkapol Saengdeejing, Ryoji Sahara & Yoshiaki Toda (2024) First-principles thermodynamic modeling for the Al-Nb-Ni ternary system, Science and Technology of Advanced Materials: Methods, 4:1, 2412968, DOI: 10.1080/27660400.2024.2412968

To link to this article: https://doi.org/10.1080/27660400.2024.2412968

Published online: 25 Nov 2024.

SCIENCE AND TECHNOLOGY OF ADVANCED MATERIALS: METHODS
2024, VOL. 4, NO. 1, 2412968
https://doi.org/10.1080/27660400.2024.2412968

First-principles thermodynamic modeling for the Al-Nb-Ni ternary system

Arkapol Saengdeejing, Ryoji Sahara and Yoshiaki Toda

Computational Structural Materials Group, Materials Evaluation Field, Research Center for Structural Materials, National Institute for Materials Science, Tsukuba, Japan

ABSTRACT

In CALPHAD methodology, used for thermodynamic database construction, the first-principles calculations based on the density functional theory have increasingly become important tool to provide an input data for assessing the thermodynamic database. As the advancement in computational power, it is evident that the first-principles calculations has become integral part for determining the thermodynamic properties of the phases within the multi-component system than the time consuming and costly experimental procedures. The alloys development process can be significantly accelerated, especially in the complex multi-component systems. With first-principles data for both end-members thermodynamic descriptions and interaction parameters, the Al-Nb-Ni ternary thermodynamic database construction can be rapidly established. Without relying on any experimental data for solid-state phases, the first-principles Al-Nb-Ni thermodynamic database can exhibits most of the features comparing with the experimental phase diagram.

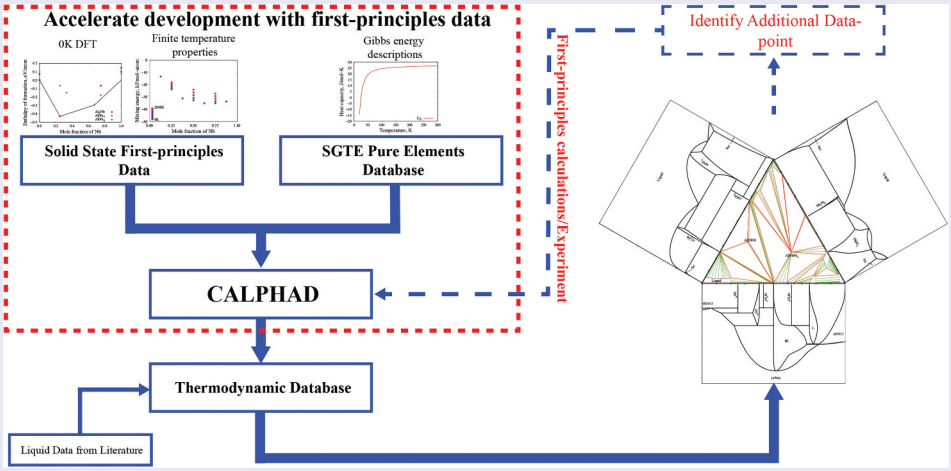

IMPACT STATEMENT

The first-principles phase diagram can reproduced most of the features presented in published experimental phase diagram. It enable rapid construction of thermodynamic database where experiments are time consuming and costly.

ARTICLE HISTORY
Received 23 April 2024
Revised 29 September 2024
Accepted 1 October 2024

KEYWORDS
CALPHAD; DFT; SQS; first-principles; thermodynamic database; Al-nb-ni

1. Introduction

Phase diagram is an important tool for both academic and commercial development of new alloys. Modern phase diagrams calculated from open source or commercialized programs are not only a figure that illustrate phase relations with respect to the variables presented along the axis in the phase diagram but also are the result of calculations based on the thermodynamic principles derived from the thermodynamic databases. CALPHAD methodology [1], where the multi-component thermodynamic database is established, has become an essential tool for alloys development since established in 1970s. Traditionally, the assessment of thermodynamic parameters are solely conducted through the collective of experimental data [2–6]. However, it is time consuming and expensive experimental procedures are required to obtain accurate thermodynamic descriptions for all phases appearing in any specific system. With the advancement in computational techniques, coupled between first-principles calculations and experimental data are

CONTACT Arkapol Saengdeejing saengdeejing.arkapol@nims.go.jp Computational Structural Materials Group, Materials Evaluation Field, Research Center for Structural Materials, National Institute for Materials Science, Tsukuba, Japan

increasingly becoming an attractive procedure to help shorten the assessment of the multi-component thermodynamic database. Enthalpy and entropy of formation of a single compound used to describe the free energy of the end-members in a complicated sublattice model are calculated by first-principles data [7,8]; the flexibility and robustness of first-principles calculations in aiding the development of the CALPHAD-type thermodynamic database is increasingly appealing. In our previous attempt, we successfully constructed the thermodynamic database of the Al-Ni-Ti ternary system by employing only first-principles calculations results [9].

In this work, the Al-Nb-Ni ternary system is chosen because Nb is an important alloying element in the Ni-based superalloys. The binary database of the Al-Nb, Al-Ni, and Nb-Ni systems are combined to create the Al-Nb-Ni ternary database. Previously, the first-principles Al-Ni binary thermodynamic database has been published [8]. Thus, there is no need to reconstruct the Al-Ni binary system. There are several published thermodynamic databases for both Al-Nb [4,10–12] and Nb-Ni [13–15] binary system but not a single one that have been assessed using only first-principles results or incorporated some of the first-principles calculations. Because there are several available literature, the data can be used for the validation of the established thermodynamic database. The Al-Nb-Niternary system have been modeled using experimental data by Du et al. [16]. The Al-Nb-Ni ternary system, as well as the Al-Ni-Ti system, are major constituent atoms of practical nickel-based superalloys. Intermetallic compounds, such as Al_3Nb and $NbNi_3$, with high melting points are expected to apply to ultrahigh-temperature materials. Therefore, the phase diagram of the Al-Nb-Ni ternary system is important for engineering purposes.

2. Methodology

The CALPHAD methodology is an approach used to calculate the thermodynamic properties, including the phase diagram, of any materials ranging from pure element to multi-component systems. The general principle of CALPHAD is to parameterize the temperature, composition, and/or pressure dependent Gibbs free energy of the individual phase using the thermochemical data, such as heat capacity, mixing energy, formation enthalpy, activity, etc., of individual phases coupled with phase equilibria data between phases [17]. Typically, the molar Gibbs free energy description of φ phases (G_m^{φ}) as a function of temperature (T) can be express as:

$$G_m^{\varphi} = a + bT + cT\ln T + dT^2 + eT^3 + fT^{-1} + \ldots \quad (1)$$

where a, b, c, d, e, and f are the fitted parameters. The function can be expanded to obtain a better fitting of the free energy description. For a pure element, at least three sets of either experimental or first-principles calculations data are required for evaluating all the parameters of the Gibbs free energy function defined in Equation 1. Entropy (S) can be derived from the following expression:

$$S = -\frac{dG}{dT} = -b - c(1+\ln T) - 2dT - 3eT^2 + fT^{-2} \quad (2)$$

Enthalpy (H) can be expressed as:

$$H = G + TS = a - cT - dT^2 - 2eT^3 + 2fT^{-1} \quad (3)$$

Finally, the heat capacity (C_p) can be derived from the first derivative to the temperature of the enthalpy:

$$C_p = \frac{dH}{dT} = -c - 2dT - 6eT^2 - 2fT^{-2} \quad (4)$$

Typically, formation enthalpy ($\Delta_F H$), entropy (S_T), and temperature dependent heat capacity ($C_p(T)$) are used to fit all the parameters of the Gibbs free energy description. For a phase with solubility, the Gibbs free energy can be described as follows:

$$G_m^{\varphi} = {}^0G_m^{\varphi} + {}^{ideal}G_{mix}^{\varphi} + {}^{ex}G_{mix}^{\varphi} \quad (5)$$

${}^0G_m^{\varphi}$ is the summation of the weighted end-member's Gibbs free energy, that is in case of binary system, it is the summation between the Gibbs free energy of pure components weighted and their respected mole fraction of each component. ${}^{ideal}G_{mix}^{\varphi}$ is the mixing energy according to W. L. Bragg et al. [18] in each phase. ${}^{ex}G_{mix}^{\varphi}$ is the excess Gibbs energy that represents the deviation from an ideal solution. The typical Gibbs energy for the binary solution phase is expressed as:

$$G_m^{\varphi} = x_A^{\varphi}\,{}^0G_A^{\varphi} + x_B^{\varphi}\,{}^0G_B^{\varphi} + RT\left(x_A^{\varphi}\ln x_A^{\varphi} + x_B^{\varphi}\ln x_B^{\varphi}\right) + {}^{ex}G_{mix}^{\varphi} \quad (6)$$

where ${}^0G_i^{\varphi}$, x_i^{φ}, and R are the molar Gibbs free energy of the i element in the φ phase, mole fraction of i element within the φ phase, and molar gas constant, respectively. To ensure that all the CALPHAD thermodynamic databases are compatible with each other, the pure element Gibbs free energies are standardized. The pure element Gibbs energy descriptions can be obtained from Dinsdale et al. [19]. A Redlich-Kister polynomial [20] is used for the excess Gibbs energy:

$${}^{ex}G_m^{\varphi} = x_A x_B \sum_{n=0}^{N} {}^nL_{A,B}^{\varphi}(x_A - x_B)^n \quad (7)$$

where ${}^nL_{A,B}^{\varphi}$ is the non-ideal interactions between A and B elements, and typically defined as:

$${}^nL_{A,B}^{\varphi} = {}^nA^{\varphi} + {}^nB^{\varphi}T + {}^nC^{\varphi}T\ln T + \ldots \quad (8)$$

where ${}^{n}A^{\varphi}$, ${}^{n}B^{\varphi}$, and ${}^{n}C^{\varphi}$ are the parameters that should be evaluated [21].

For the intermediate compounds with solubility, the free energy is described using compound energy formalism (CEF) [22]. The end-member free energy is formulated using Neumann-Kopp rule [23]:

$$ {}^{0}G_{m}^{A_iB_j} = i^{0}G_{m}^{A} + j^{0}G_{m}^{B} + \Delta_F H - T\Delta_F S \quad (9) $$

where ${}^{0}G_{m}^{A_iB_j}$, $\Delta_F H$, and $\Delta_F S$ are molar Gibbs free energy of A_iB_j structure, formation enthalpy, and formation entropy, respectively.

Thermo-Calc Software [24] is used for thermodynamic database construction and assessment.

2.1. First-principles calculations

The first-principles calculations, based on the density functional theory (DFT), are performed to obtain the data needed for the CALPHAD thermodynamic database assessment. In this work, all the calculations were conducted using the Vienna Ab initio Simulation Package (VASP) [25,26]. The electron-ion interactions are described using the projector augmented wave (PAW) method [27]. The generalized gradient approximation (GGA) of Perdew-Burke-Ernzerhof (PBE) [28] is selected to describe the exchange and correlation energy. The PAW potential sets are comprised of a $2p^1 2s^2$ configurations of valance electron for Al, $4p^6 5s^1 4d^4$ for Nb and $3d^{10}$ for Ni. All the calculations are performed with spin polarized enable. For the total energy calculations, the k-point mesh of Γ-centered Monkhorst-Pack [29] is used for integration of the Brillouin zone during both structure relaxations and final static calculations. The 1^{st} order Methfessel-Paxton smearing method [30] is used for with a 0.2 eV temperature broadening parameter for the electronic occupation. To obtain highly accurate energy and density of states (DOS) during the final static calculation, the Blöchl correction linear tetrahedron method [31] is performed. Table 1 lists k-points meshes for each structure. Each k-point mesh is selected to ensure that convergence of the electronic energies is lower than 0.1 meV. All the calculations were performed with the cutoff energy of 500 eV.

The Helmholtz free energy as a function of volume (V) and temperature of a single structure ($F(V,T)$) can be partitioned into the different contributions, such as ground state energy ($E_{0K}(V)$), thermal electron excitation ($F_{el}(V,T)$), and vibrational contribution ($F_{vib}(V,T)$):

$$ F(V,T) = E_{0K}(V) + F_{el}(V,T) + F_{vib}(V,T) \quad (10) $$

The formation enthalpy for each end-member is calculated using the following formula:

$$ \Delta_f H = E_0^{A_aB_b} - \sum_i x_i E_0^i \quad (11) $$

where $E_0^{A_aB_b}$ is the 0K energy of the A_aB_b end-member with number of a and b atoms, x_i is the mole fraction of element i, and E_0^i is the 0K energy of i element in their stable structure at 298.15 K.

In CALPHAD, instead of Helmholtz energy, Gibbs energy is primarily used. Using Legendre transformation, the Gibbs free energy ($G(P,T)$) is expressed as:

$$ G(P,T) = F(V,T) - \left(\frac{\partial F}{\partial V}\right)_T V \quad (12) $$

The contribution to the free energy from thermal electron excitation (F_{el}) where the energy emerge from the random occupancy of thermally excited electron in the energy level above Fermi energy is calculated using the following equation [32]:

$$ F_{el}(V,T) = E_{el}(V,T) - TS_{el}(V,T) \quad (13) $$

$$ E_{el}(V,T) = \int n(\varepsilon,V) f(\varepsilon,T)\varepsilon d\varepsilon - \int^{\varepsilon F} n(\varepsilon,V)\varepsilon d\varepsilon \quad (14) $$

$$ S_{el}(V,T) = -k_B \int n(\varepsilon,V)[f(\varepsilon,T)\ln f(\varepsilon,T) + (1-f(\varepsilon,T))\ln(1-f(\varepsilon,T))]d\varepsilon \quad (15) $$

where $E_{el}(V,T)$ is the thermal electron excitation energy, $n(\varepsilon,V)$ is the electronic density of states (DOS) at ε energy, S_{el} is the bare electronic entropy, ε_F is Fermi energy, k_B is Boltzmann constant, and f is Fermi distribution function:

$$ f(\varepsilon,T) = \frac{1}{\exp\left(\frac{\varepsilon-\mu_e}{k_B T}\right)+1} \quad (16) $$

where μ_e is the electron chemical potential, which is equivalent to the Fermi energy at 0 K.

Vibrational contribution ($F_{vib}(V,T)$) is corresponded to the lattice vibration energy and calculated through the phonon density of states (PDOS). Supercell method, as implemented in the Alloy Theoretical Automated Toolkit (ATAT) [33], are used for the PDOS calculations. The minimum separation between perturbed atoms are set to be approximately 10–12 Å to ensure that the interference from perturbed atom are isolated from the same perturbed atom from periodic boundary condition. The 0.1 Å displacement for each perturbed atom is selected for the phonon calculations. For better accuracy in force constant matrix calculation during the phonon calculations, the 1^{st} order Methfessel-Paxton is used. In this work, quasi-harmonic phonon approximation is not considered, and only harmonic phonon approximation is performed to reduce the computational time. The lattice vibrational contribution is calculated from the following equation [34]:

Table 1. Formation enthalpy, formation entropy and correspond k-point mesh for all structures used in this work and from published thermodynamic databases (in parenthesis).

		Formation energy		
Structures	Compositions	$\Delta_F H$, kJ/mol	$\Delta_F S$, J/mol-K	k-point mesh
Al_3Nb	Al_4	0.00	0.00	13×13x15
	Al_3Nb	−41.52(−41.75[a])	−7.14	
	Al_3Ni	−21.02	3.14	
	Nb_3Al	−6.33	−0.27	
	Nb_4	13.97	−1.47	
	Nb_3Ni	9.20	2.85	
	Ni_3Al	−39.10	0.16	
	Ni_3Nb	−27.71	−19.79	
	Ni_4	0.00	0.00	
$AlNb_2$	Al_{30}	6.44	4.44	7×7x7
	$Al_{10}Nb_{20}$	−28.67(−26.77[a])	−4.88	
	$Al_{10}Ni_{20}$	−31.64	−3.27	
	$Nb_{10}Al_{20}$	−14.54	−1.85	
	Nb_{30}	8.03	−1.06	
	$Nb_{10}Ni_{20}$	4.65	5.29	
	$Ni_{10}Al_{20}$	−30.89	2.37	
	$Ni_{10}Nb_{20}$	−10.51	0.59	
	Ni_{30}	9.59	4.59	
$AlNb_3$	Al_8	7.61	6.04	11×11x11
	Al_2Nb_6	−17.46(−19.59[a])	4.19	
	Al_2Ni_6	−25.84	0.18	
	Nb_2Al_6	−6.39	−2.12	
	Nb_8	10.14	2.22	
	Nb_2Ni_6	−21.46	4.33	
	Ni_2Al_6	−23.14	5.04	
	Ni_2Nb_6	−5.33	1.10	
	Ni_8	13.22	6.96	
$NbNi_3$	Al_8	3.17	0.00	11×11x11
	Al_2Nb_6	−9.93	−3.08	
	Al_2Ni_6	−39.52	−2.65	
	Nb_2Al_6	−32.10	−6.18	
	Nb_8	19.04	0.55	
	Nb_2Ni_6	−28.47(−30.80[b])	−0.53	
	Ni_2Al_6	−24.81	0.20	
	Ni_2Nb_6	11.13	4.12	
	Ni_8	2.38	0.91	
Nb_7Ni_6	Al_{39}	10.34	5.18	7×7x7
	$Al_{18}Nb_{21}$	−24.03	−3.83	
	$Nb_{18}Al_{21}$	2.55	1.71	
	$Nb_{18}Nb_{21}$	16.64	−0.90	
	$Ni_{18}Al_{21}$	−45.72	0.32	
	$Ni_{18}Nb_{21}$	−19.96(−21.96[b])	−0.50	
$NbNi_8$	$NbNi_8$	−12.44(−14.28[b])	−0.01	11×11x7
$AlNbNi_2$	$AlNbNi_2$	−42.06(−76.19[c])	4.00	13×13x13
AlNbNi	$Al_8Nb_8Al_8$	−28.25(−11.24[c])	−4.68	9×7x7
	$Al_8Nb_8Ni_8$	−41.50	−3.22	
	$Ni_8Nb_8Al_8$	−38.55	−2.88	
	$Ni_8Nb_8Ni_8$	−18.76(−25.70[c])	−1.00	

[a] He et al. [12].
[b] Chen et al. [15].
[c] Du et al. [16].

$$F_{vib}(V,T) = k_B T \int_0^\infty \ln\left[2\sinh\frac{\hbar\omega}{2k_B T}\right] g(\omega) d\omega \quad (17)$$

where $\hbar$, ω, and $g(\omega)$ are the reduced Planck constant, phonon frequencies, and PDOS, respectively.

A disordered configuration in the solution phase is obtained using a special quasi-random structure (SQS) [35] based on cluster expansion method (CEM) [36]. The mixing energy of the fcc, bcc, and hcp lattice is calculated from the SQSs at 12.5, 25, 37.5, 50, 62.5, 75, and 87.5 at.%. The mixing energy ($\Delta_{mix}G$)) is calculated by the following equation:

$$\Delta_{mix}G^{\varphi}_{SQS} = G^{\varphi}_{SQS} - x_A G^{\varphi}_A - x_B G^{\varphi}_B \quad (18)$$

where G^{φ}_i is the Gibbs free energy of i element in φ structure. Additional SQSs have been generated to represent the mixing energy of the different elements in the sublattice of intermediate compounds. The calculated correlation functions of Al_3(Al,Nb) SQS are listed in Table 2. Up to the 9^{th} pairs of the Al_3(Al,Nb) SQS pair correlation functions are perfectly allied with the pair correlation functions of theoretical random configuration and all 10^{th} three-body clusters (triple) are matched. In this work, the calculated correlation functions of all SQSs, up to at least 6^{th} pair and 4^{th} triplet, are perfectly matched with the theoretical random correlation functions of the

Table 2. Correlation function of $Al_3(Al_{0.5},Nb_{0.5})$ SQS compared with theoretical random configuration.

Cluster type	Cluster size, Å	Correlation function	
		Calculated	Random
Pair	3.8520	0.0000	0.0000
	5.1075	0.0000	0.0000
	5.4476	0.0000	0.0000
	7.4674	0.0000	0.0000
	7.7040	0.0000	0.0000
	8.6134	0.0000	0.0000
	8.6411	0.0000	0.0000
	9.2433	0.0000	0.0000
	9.4608	0.0000	0.0000
	10.2149	−0.5000	0.0000
	10.7291	0.0000	0.0000
	10.8952	0.0000	0.0000
Triplet	5.1075	0.0000	0.0000
	5.4476	0.0000	0.0000
	5.4476	0.0000	0.0000
	7.4674	0.0000	0.0000
	7.4674	0.0000	0.0000
	7.4674	0.0000	0.0000
	7.4674	0.0000	0.0000
	7.7040	0.0000	0.0000
	7.7040	0.0000	0.0000
	7.7040	0.0000	0.0000

same composition. The details of all generated SQSs are listed in Table 3.

In this work, short-range ordering contribution and state-of-the-art approaches for liquid free energy calculations are not considered owing to the limited computational resources. We discussed the short-range ordering and state-of-the-art liquid calculations in our previously published work [9].

3. Results and discussions

3.1. Al-Ni

The thermodynamic descriptions for the Al-Ni binary system is taken from Davey et al. [8]. The bcc and fcc two sublattice model will be used instead of the original four sublattice model. All other parameters remain unchanged. Figure 1 shows the Al-Ni binary phase diagram calculated using two sublattice model for both fcc and bcc phases.

3.2. Al-Nb

According to the data presented in the Materials Project database [40], there are four existing compounds but only three are experimentally observed, which are $AlNb_2$, $AlNb_3$, and Al_3Nb. To model the solubility of all three structures, the two sublattice model will be implemented for all intermediate phases. Table 4 shows details of crystal structures for all compounds. $(Al,Nb)_3(Al,Nb)$, $(Al,Nb)(Al,Nb)_2$, and $(Al,Nb)(Al,Nb)_3$ sublattice models are implemented to describe the solid solubility for all three phases in the binary system. To reduce the complexity of the calculations, $(Al,Nb)(Al,Nb)_2$ sublattice model is chosen instead of more complex $(Al,Nb)_5Nb_2(Al,Nb)_8$, which can correctly represent the solid solubility in the σ phase. Table 4 lists the sublattice model used for the Al-Nb binary system. Figure 2 shows the calculated Gibbs energy of formation as a function of temperature for Al_3Nb, $AlNb_2$, and $AlNb_3$. It can be observed that the Gibbs energy of formations are fairly linear at the elevated temperature. Therefore, we can use Equation 9 to approximate the Gibbs free energy of all the end-members. Using linear regression fitting, the slope of the plot in Figure 2 is approximated as the negative of entropy of formation. Table 1 lists all the calculated formation enthalpy and entropy for all the end-member structures required to represent sublattice model of all three phases in the Al-Nb binary system.

Table 3. Mixing site, compositions, and size of all SQSs used in this work.

Structures	Mixing site	SQS composition	No. atoms	Ref.
fcc	$(A_{0.875}B_{0.125})$	$A_{56}B_8$	64	[8]
	$(A_{0.75}B_{0.25})$	$A_{12}B_4$	16	[37]
	$(A_{0.625}B_{0.375})$	$A_{40}B_{24}$	64	[8]
	$(A_{0.5}B_{0.5})$	A_8B_8	16	[37]
bcc	$(A_{0.875}B_{0.125})$	$A_{56}B_8$	64	[8]
	$(A_{0.75}B_{0.25})$	$A_{12}B_4$	16	[38]
	$(A_{0.625}B_{0.375})$	$A_{40}B_{24}$	64	[8]
	$(A_{0.5}B_{0.5})$	A_8B_8	16	[38]
hcp	$(A_{0.875}B_{0.125})$	$A_{56}B_8$	64	[8]
	$(A_{0.75}B_{0.25})$	$A_{12}B_4$	64	[39]
	$(A_{0.625}B_{0.375})$	$A_{40}B_{24}$	64	[8]
	$(A_{0.5}B_{0.5})$	A_8B_8	64	[39]
Al_3Nb	$A_3(A_{0.5}B_{0.5})$	$A_{56}B_8$	64	This work
$AlNb_2$	$(A_{1/3}B_{2/3})_3$	$A_{90}B_{180}$	270	This work
$AlNb_3$	$(A_{0.5}B_{0.5})B_3$	A_8B_{56}	64	This work
Nb_7Ni_6	$A_7(A_{0.5}B_{0.5})_6$	$A_{120}B_{36}$	156	This work
$NbNi_3$	$(A_{0.5}B_{0.5})B_3$	A_8B_{56}	64	This work
	$A(A_{0.5}B_{0.5})_3$	$A_{40}B_{24}$	64	This work
	$(A_{0.5}B_{0.5})C_3$	$A_8B_8C_{48}$	64	This work
$L1_2$	$(A_{0.5}B_{0.5})B_3$	A_8B_{56}	64	This work
	$A(A_{0.5}B_{0.5})_3$	$A_{40}B_{24}$	64	This work
	$(A_{0.5}B_{0.5})C_3$	$A_8B_8C_{48}$	64	This work
AlNbNi	$(A_{0.5}C_{0.5})BC$	$A_8B_{16}C_{24}$	48	This work
	$AB(A_{0.5}C_{0.5})$	$A_8B_{16}C_{24}$	48	This work
	$(A_{0.5}C_{0.5})B(A_{0.5}C_{0.5})$	$A_{16}B_{16}C_{16}$	48	This work

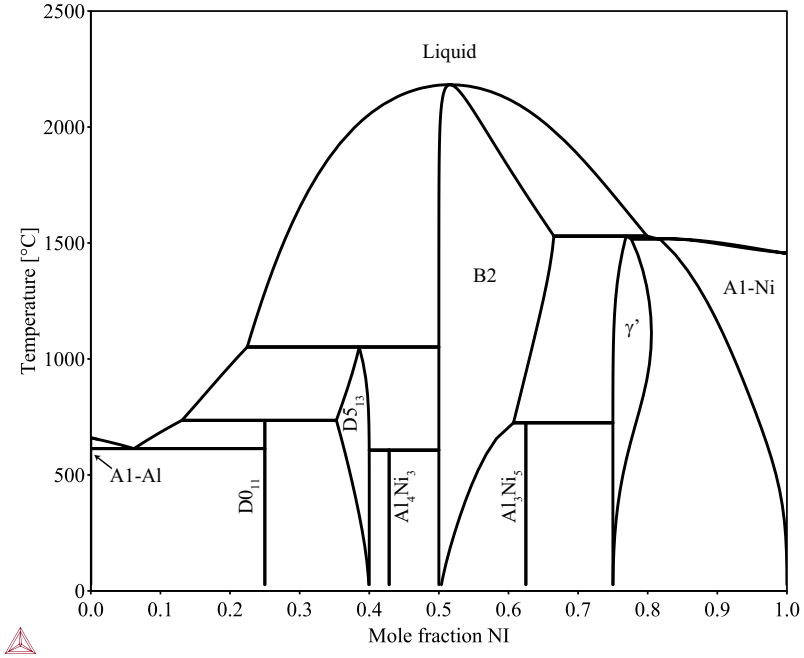

Figure 1. First-principles phase diagram of the Al-Ni binary system [8].

Table 4. Information about crystal symmetry, lattice parameters, and CALPHAD sublattice model for all compounds appear in this work.

						Lattice parameter						
Phases	Prototypes	Pearson	SG	# atom	Models	a	b	c	α	β	γ	Ref.
Al_3Nb	Al_3Ti	tI8	I4/mmm	4	$(Al,Nb,Ni)_3(Al,Nb,Ni)$	5.1075	5.1075	5.1075	136	136	64	[41]
$AlNb_2$ (σ)	$(Cr_{0.5}Fe_{0.5})$	tP30	$P4_2/mmm$	30	$(Al,Nb,Ni)(Al,Nb,Ni)_2$	10.0028	10.0028	5.2014	90	90	90	[10]
$AlNb_3$	Cr_3Si	cP8	$Pm\bar{3}n$	8	$(Al,Nb,Ni)(Al,Nb,Ni)_3$	5.2133	5.2133	5.2133	90	90	90	[42]
$NbNi_3$	Cu_3Ti	oP8	Pmmn	8	$(Al,Nb,Ni)(Al,Nb,Ni)_3$	4.2560	4.5616	5.1240	90	90	90	[43]
Nb_7Ni_6 (μ)	Fe_7W_6	hR39	$R\bar{3}m$	39	$(Al,Nb)_7(Al,Nb,Ni)_6$	4.9436	4.9436	27.0921	90	90	120	[64]
$NbNI_8$	V_4Zn_5	tI18	I4/mmm	9	$NbNi_8$	5.6739	5.6739	5.6739	96	96	143	[44]
$AlNbNi_2$	$AlCu_2Mn$	cF16	$Fm\bar{3}m$	4	$AlNbNi_2$	4.2460	4.2460	4.2460	60	60	60	[45]
AlNbNi	$MgZn_2$	hP12	$P6_3/mmc$	24	(Al,Ni)Nb(Al,Ni)	5.0545	8.4908	8.0346	90	90	90	[46]

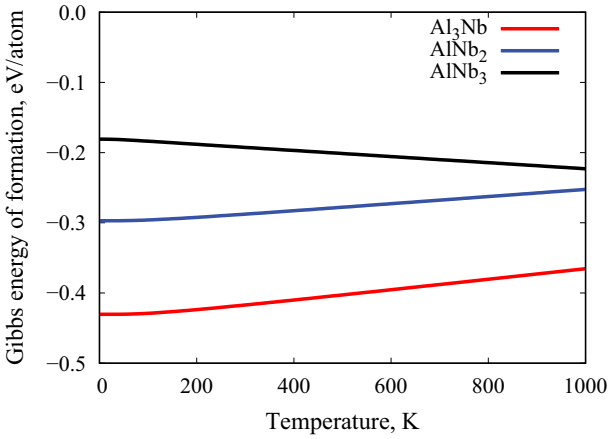

Figure 2. Gibbs energy of formation as a function of temperature for Al_3Nb, $AlNb_2$, and $AlNb_3$ compounds.

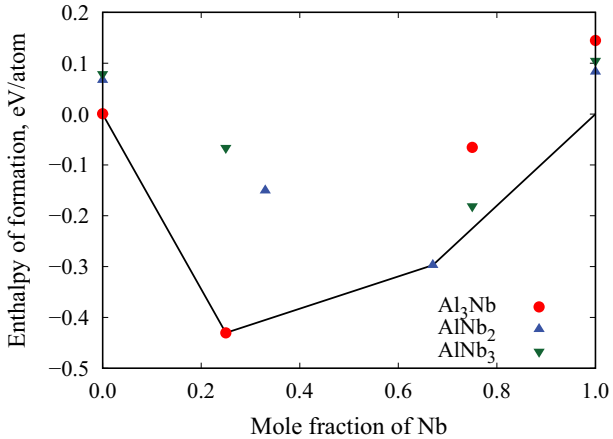

Figure 3. Formation enthalpy for binary compounds and their corresponding end-members of sublattice model, $(Al,Nb)_3(Al,Nb)$, $(Al,Nb)(Al,Nb)_2$, and $(Al,Nb)(Al,Nb)_3$, with connected convex hull of the Al-Nb binary system.

Figure 3 illustrates the formation enthalpy for all three structures, including their anti-site configurations. The solid line represents the convex hull where the lowest possible energy of any combinations for all the structures exists in the Al-Nb binary system. In experimental phase diagram [10], all three phases (Al_3Nb, $AlNb_2$, and $AlNb_3$) are stable but only for data available above 500 °C. The calculated formation

energy of $AlNb_3$ is above the convex hull. Experimental measurement and estimation for the enthalpy of formations at 298.15 K ($\Delta_F H^\circ$) show some discrepancy for the stability of $AlNb_3$ phase [47–52]. The recent enthalpy of formation measurement shows that $AlNb_3$ is not formed in the convex hull [50]. The published thermodynamic database based on experimental assessment listed the enthalpy of formation of $AlNb_3$ end-member at 298.15 K above the convex hull. Because there are no experimentally verification of $AlNb_3$ stability at considerably low temperature (below 0 °C), we can assume that $AlNb_3$ is unstable at 0 K. Table 1 shows the enthalpy of formation of stable compounds obtained from the published thermodynamic database [12] in parenthesis. The differences between the enthalpies of formation calculated from the DFT and the values extracted from the assessed thermodynamic database are typically within ±3 kJ/mol of each other. According to the sublattice models that represent the solid solution of all three intermediate compounds in Al-Nb binary system, 5 types of binary interaction parameters, for example (Al_3Nb), ${}^nL^{Al_3Nb}_{(Al,Nb)_3Al}$, ${}^nL^{Al_3Nb}_{(Al,Nb)_3Nb}$, ${}^nL^{Al_3Nb}_{Al_3(Al,Nb)}$, ${}^nL^{Al_3Nb}_{Nb_3(Al,Nb)}$, ${}^nL^{Al_3Nb}_{(Al,Nb)_3(Al,Nb)}$, are available for each sublattice model. Not all the interaction parameters will be significantly affected on the solubility of the solution phases. The SQSs are generated according to the selected interaction parameters. The SQS with the equiatomic configurations within the sublattice will be used for obtaining mixing energy, which will be used to evaluate the interaction parameters. Table 3 lists the generated SQSs for the Al-Nb binary system.

Table 5 lists the calculated enthalpy of mixing of the SQSs for Al-Nb binary system. We encountered a convergence problem while calculating the energy of $AlNb_2$ SQS. Thus, the mixing energy of $AlNb_2$ SQS is currently unavailable. The interaction parameters within each sublattice model will be evaluated based on the calculated enthalpy of mixing with the assumption of regular solution (only 0^{th} interaction parameter is used). The interaction parameter can be directly obtained from the following equation:

$$\Delta_{mix}G_{SQS} = x_i x_j \left({}^0A_{i:j} + {}^0B_{i:j}T\right) \tag{19}$$

Within the regular solution model, the temperature dependent interaction parameter will not be obtained owing to the computational expensive of the SQS for finite temperature properties.

For disordered phase, the mixing energy calculated from first-principles calculations corresponded to the excess term presented in Equation 5. For simplicity, only 0^{th}-ordered interaction parameter will be used. Both temperature independent and dependent terms in the interaction parameters are fitted through the Equation 19. Figure 4 shows calculated SQS enthalpy of mixing (0 K) across the composition range for fcc, bcc, and hcp structures. There are some anomaly with the results, especially at higher at.% Nb in fcc and hcp lattice. The mixing enthalpy seems to be more stable compared to the lower at.% Nb. The mixing enthalpy at 50 at.% Nb of bcc and hcp seem to be significantly more stable than that at 37.5 and 62.5 at.% Nb. This can occurred when relaxing the atomic position of the SQS by DFT, especially when the atomic size between two mixing elements are moderately different. The SQS, which should represent the disordered

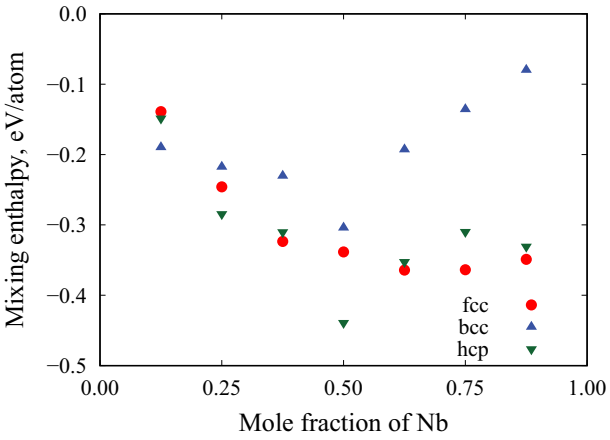

Figure 4. Mixing enthalpy of fcc-, bcc-, and hcp-disordered phases from SQS for the Al-Nb binary system.

Table 5. Mixing enthalpy of SQS for interaction parameters evaluation.

Mixing structures	SQS composition	Mixing enthalpy, eV/atom
$Al_3(Al,Nb)$-Al_3Nb	$Al_{56}Nb_8$	0.0507
$(Al,Nb)(Al,Nb)_2$	$Al_{90}Nb_{180}$	N/A
$(Al,Nb)Nb_3$-$AlNb_3$	Al_8Nb_{56}	0.0532
$(Nb,Ni)Ni_3$-$NbNi_3$	Nb_8Ni_{56}	0.0201
$Nb(Nb,Ni)_3$-$NbNi_3$	$Nb_{40}Ni_{24}$	0.0441
$Nb_7(Nb,Ni)_6$-Nb_7Ni_6	$Nb_{120}Ni_{36}$	N/A
$(Al,Nb)Ni_3$-$L1_2$	$Al_8Nb_8Ni_{48}$	−0.0938
$(Al,Ni)Ni_3$-$L1_2$	Al_8Ni_{56}	0.0123
$Nb(Nb,Ni)_3$-$L1_2$	$Nb_{40}Ni_{24}$	−0.0999
$(Al,Nb)Ni_3$-$NbNi_3$	$Al_8Nb_8Ni_{48}$	0.0113
(Al,Ni)NbNi-AlNbNi	$Al_8Nb_{16}Ni_{24}$	−0.0267
AlNb(Al,Ni)-AlNbNi	$Al_{24}Nb_{16}Ni_8$	−0.0940
(Al,Ni)Nb(Al,Ni)-AlNbNi	$Al_{16}Nb_{16}Ni_{16}$	−0.1773

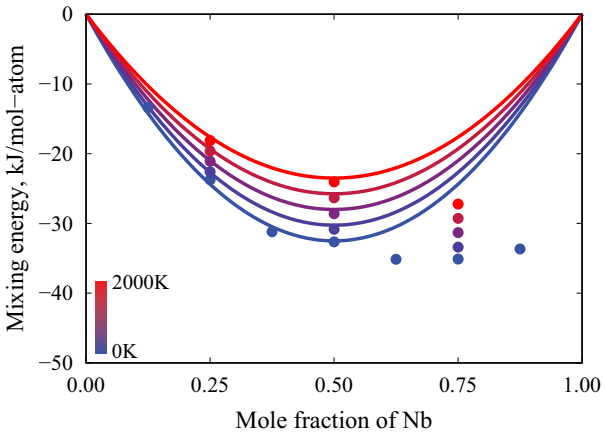

Figure 5. Finite temperature mixing energy of the Al-Nb fcc-disordered SQS (point) with CALPHAD excess energy from fitted interaction parameters using the mixing energy (line).

configuration, tends to collapse into ordered structure. By comparing the calculated radial distribution function (RDF) between collapsed SQS and initial disordered structure, it usually shows largely deviation from the initial disordered structure. Further discussion about this problem is presented in our previous work [9]. If any calculated SQSs show both abnormally enthalpy of mixing and the deviation from the initial structure RDF, we excluded all the anomaly results from the interaction parameters evaluations. Finite temperature phonon calculations were performed on SQSs to obtain the vibrational contribution to the free energy. The total free energy can be obtained from combining 0K, electron excitation, and vibrational contributions as presented in Equation 10. Figure 5 shows finite temperature mixing energy of fcc SQS at 0, 500, 1000, 1500 and 2000 K. Only the finite temperature at 25, 50 and 75 at.% Nb were obtained owing to the higher computational resource required at other concentration. Only the data from 12.5 to 50 at.% Nb were excluded owing to the anomaly mention earlier. With these data points, temperature dependent interaction parameters were evaluated according to Equation 7. The solid lines in Figure 5 show the calculated excess term at 0, 500, 1000, 1500 and 2000 K from the interaction parameters listed in Table 6.

Figure 6 shows the Al-Nb binary phase diagram calculated from the first-principles data. The liquid interaction parameters are all equal to zero, corresponds to an ideal solution model. The $AlNb_2$ only stabilize up to 730 °C. As aforementioned, $AlNb_3$ is unstable at 0 K. The stability of $AlNb_3$ begins from 240 °C. Without the liquid interaction parameters, $AlNb_3$ stability is extended to high temperature. Even with the ideal solution for the liquid phase, the calculated Al-Nb phase diagram exhibits all the distinguish features similar to the calculated phase diagram from He et al. [12] as shown in Figure 7. At the temperature above 3500 °C, bcc-disordered phase become stable again. It it typical to see this kind of behavior occurs in assessed thermodynamic database. Owing to the limited number of terms used in the interaction parameters, result in the incorrect extrapolation in the high temperature region. Thus, we adjust the liquid interaction parameters based on the data from Witusiewicz et al. [11]. The Al-Nb liquid interaction parameters are listed in Table 6. Figure 8 illustrates the Al-Nb binary phase diagram calculated with the interaction parameters of the liquid phase listed in Table 6. All the features that comparable with the calculated phase diagram from He et al. [12] are presented in the calculated phase diagram. In published phase diagram, the decomposition of both $AlNb_2$ and $AlNb_3$ are from peritectic reaction; however, in our calculated phase diagram, $AlNb_2$ in not decompose into liquid phase owing to the lower stability of $AlNb_2$ phase. $AlNb_3$ is melting congruently instead of peritectic reaction. It is possibly from the lower liquid stability at high temperature from the liquid interaction parameters. By adjusting the liquid interaction parameters, it is possible to achieve the peritectic reaction for the $AlNb_3$ decomposition. At high temperature, the bcc-disordered phase boundary is deviated from He et al. [12] phase diagram. It is likely owing to the simplification of the bcc-disordered interaction parameters. Because only 0^{th}-ordered parameter is used, where He el al. [12] used both 0^{th}- and 1^{st}-ordered interaction parameters. To accurately represent the bcc-disordered phase boundary at high temperature, more interaction parameters and accurate DFT calculations might needed.

3.3. Nb-Ni

According to Materials Project database [40], there are only two stable intermediate compounds (Nb_7Ni_6 and $NbNi_3$). However, based on experimental data [53–56], there is one more stable compound ($NbNi_8$). According to the literature, $NbNi_8$ is stable from low temperature and decomposed via peritectoid reaction into $NbNi_3$ and fcc-disordered at 515 °C. There is no report of solid solubility in $NbNi_8$. Thus, the stoichiometric description will be used for $NbNi_8$ phase. Nb_7Ni_6 and $NbNi_3$ phases appear to have solid solubility. To accommodate the solid solubility in $NbNi_3$, $(Nb,Ni)(Nb,Ni)_3$ sublattice will be employed. Nb_7Ni_6 is typically called μ phase. To correctly model the solubility in Nb_7Ni_6 phase, a four sublattice model $((Nb,Ni)Nb_4(Nb,Ni)_2(Nb,Ni)_6)$ is required. However,

Table 6. CALPHAD parameters for the Al-Nb-Ni thermodynamic database (part 1).

Phases	Gibbs/Interactions	Parameters
fcc	${}^{0}G_{Al}^{fcc}$	${}^{a0}G_{Al}^{fcc}$
	${}^{0}G_{Nb}^{fcc}$	${}^{a0}G_{Nb}^{fcc}$
	${}^{0}G_{Ni}^{fcc}$	${}^{a0}G_{Ni}^{fcc}$
	${}^{0}L_{Al,Nb}^{fcc}$	− 130000 + 18T
	${}^{0}L_{Al,Ni}^{fcc}$	− 145582 + 8.17T [8]
	${}^{1}L_{Al,Ni}^{fcc}$	+59552 - 4.7T [8]
	${}^{2}L_{Al,Ni}^{fcc}$	+65528 - 2.29T [8]
	${}^{0}L_{Nb,Ni}^{fcc}$	− 75000
bcc	${}^{0}G_{Al}^{bcc}$	${}^{a0}G_{Al}^{bcc}$
	${}^{0}G_{Nb}^{bcc}$	${}^{a0}G_{Nb}^{bcc}$
	${}^{0}G_{Ni}^{bcc}$	${}^{a0}G_{Ni}^{bcc}$
	${}^{0}L_{Al,Nb}^{bcc}$	− 75000 + 18T
	${}^{0}L_{Al,Ni}^{bcc}$	− 93693 + 6T [8]
	${}^{1}L_{Al,Ni}^{bcc}$	+82380 - 7T [8]
	${}^{2}L_{Al,Ni}^{bcc}$	+87090 - 4.95T [8]
	${}^{0}L_{Nb,Ni}^{bcc}$	− 12250 + 3.5T
hcp	${}^{0}G_{Al}^{hcp}$	${}^{a0}G_{Al}^{hcp}$
	${}^{0}G_{Nb}^{hcp}$	${}^{a0}G_{Nb}^{hcp}$
	${}^{0}G_{Ni}^{hcp}$	${}^{a0}G_{Ni}^{hcp}$
	${}^{0}L_{Al,Nb}^{hcp}$	− 140000 + 23T
Liquid	${}^{0}G_{Al}^{liq}$	${}^{a0}G_{Al}^{liq}$
	${}^{0}G_{Nb}^{liq}$	${}^{a0}G_{Nb}^{liq}$
	${}^{0}G_{Ni}^{liq}$	${}^{a0}G_{Ni}^{liq}$
	${}^{0}L_{Al,Nb}^{liq}$	− 110000 + 20T
	${}^{1}L_{Al,Nb}^{liq}$	+8500
	${}^{0}L_{Al,Ni}^{liq}$	− 207109 + 41.32T [8]
	${}^{1}L_{Al,Ni}^{liq}$	− 10186 + 5.87T [8]
	${}^{2}L_{Al,Ni}^{liq}$	+81205 - 31.96T [8]
	${}^{3}L_{Al,Ni}^{liq}$	+4365 - 2.52T [8]
	${}^{4}L_{Al,Ni}^{liq}$	− 22102 + 13.16T [8]
	${}^{0}L_{Nb,Ni}^{liq}$	− 80000 - 6.3T
	${}^{1}L_{Nb,Ni}^{liq}$	+100000 - 19T
	${}^{3}L_{Nb,Ni}^{liq}$	+10000
Al_3Nb	${}^{0}G_{Al_4}^{Al_3Nb}$	$4\ {}^{a0}G_{Al}^{fcc}$ +1000 + T
	${}^{0}G_{Al_3Nb}^{Al_3Nb}$	$3\ {}^{a0}G_{Al}^{fcc} + {}^{a0}G_{Nb}^{bcc}$ − 166076 + 28.56T
	${}^{0}G_{Nb_3Al}^{Al_3Nb}$	${}^{a0}G_{Al}^{fcc} + 3\ {}^{a0}G_{Nb}^{bcc}$ − 25301 + 1.07T
	${}^{0}G_{Nb_4}^{Al_3Nb}$	$4\ {}^{a0}G_{Nb}^{bcc}$ +55883 + 5.9T
	${}^{0}L_{Al:Al,Nb}^{Al_3Nb}$	+20000
	${}^{0}L_{Al,Nb:Nb}^{AlNb_3}$	+20000
$AlNb_2$	${}^{0}G_{Al_3}^{AlNb_2}$	$3\ {}^{a0}G_{Al}^{fcc}$ +19326 - 13.33T
	${}^{0}G_{AlNb_2}^{AlNb_2}$	${}^{a0}G_{Al}^{fcc} + 2\ {}^{a0}G_{Nb}^{bcc}$ − 86001 + 14.63T
	${}^{0}G_{AlNi_2}^{AlNb_2}$	${}^{a0}G_{Al}^{fcc} + 2\ {}^{a0}G_{Ni}^{fcc}$ − 94927 + 9.82T
	${}^{0}G_{NbAl_2}^{AlNb_2}$	$2\ {}^{a0}G_{Al}^{fcc} + {}^{a0}G_{Nb}^{bcc}$ − 43614 + 5.56T
	${}^{0}G_{Nb_3}^{AlNb_2}$	$3\ {}^{a0}G_{Nb}^{bcc}$ +24080 + 3.19T
	${}^{0}G_{NbNi_2}^{AlNb_2}$	${}^{a0}G_{Nb}^{bcc} + 2\ {}^{a0}G_{Ni}^{fcc}$ +13964 - 15.88T
	${}^{0}G_{NiAl_2}^{AlNb_2}$	$2\ {}^{a0}G_{Al}^{fcc} + {}^{a0}G_{Ni}^{fcc}$ − 92670 - 7.10T
	${}^{0}G_{NiNb_2}^{AlNb_2}$	$2\ {}^{a0}G_{Nb}^{bcc} + {}^{a0}G_{Ni}^{fcc}$ − 31522 - 1.76T
	${}^{0}G_{Ni_3}^{AlNb_2}$	$3\ {}^{a0}G_{Ni}^{fcc}$ +28756 - 13.77T

[a] SGTE pure elements database [19].

to reduce to complexity of the sublattice model and shorten the calculation times, $Nb_7(Nb,Ni)_6$ sublattice model is selected to represent the solubility between Nb and Ni for Nb_7Ni_6 phase. Only Ni site can be occupied with Nb atom but Nb site cannot be occupied by Ni atom. Table 4 lists the sublattice model used for the Nb-Ni binary system. Chen et al. [15] also selected $Nb_7(Nb,Ni)_6$ sublattice model to represent the solubility in the Nb_7Ni_6 phase. The calculated DFT results for all the end-member structures in the Nb-Ni binary system are listed in Table 1.

Figure 9 plots all the calculated formation enthalpy at different Ni concentration for all two structures, including their anti-site configurations. There are only two structures that formed the convex hull (Nb_7Ni_6 and $NbNi_3$). The enthalpy of formation for

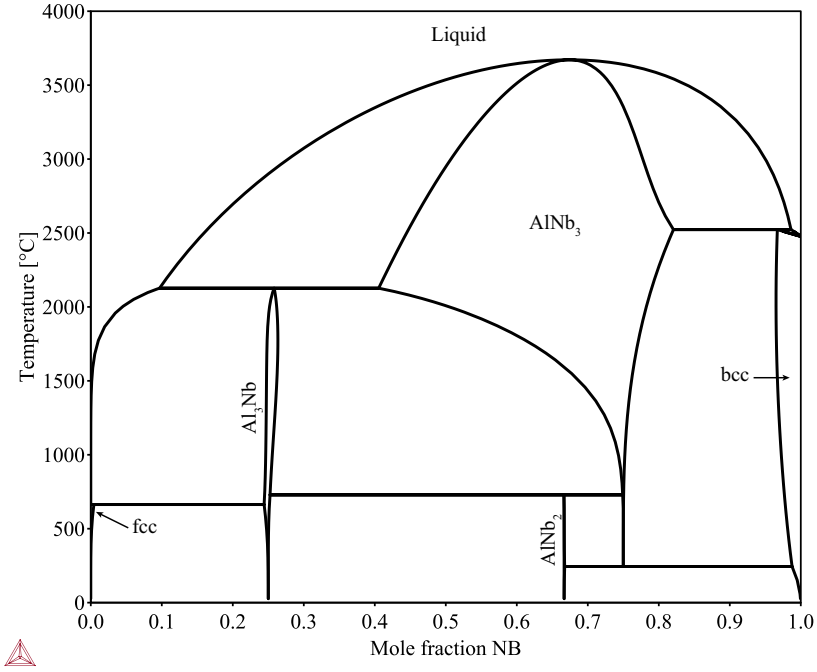

Figure 6. Phase diagram of the Al-Nb binary system with ideal liquid model.

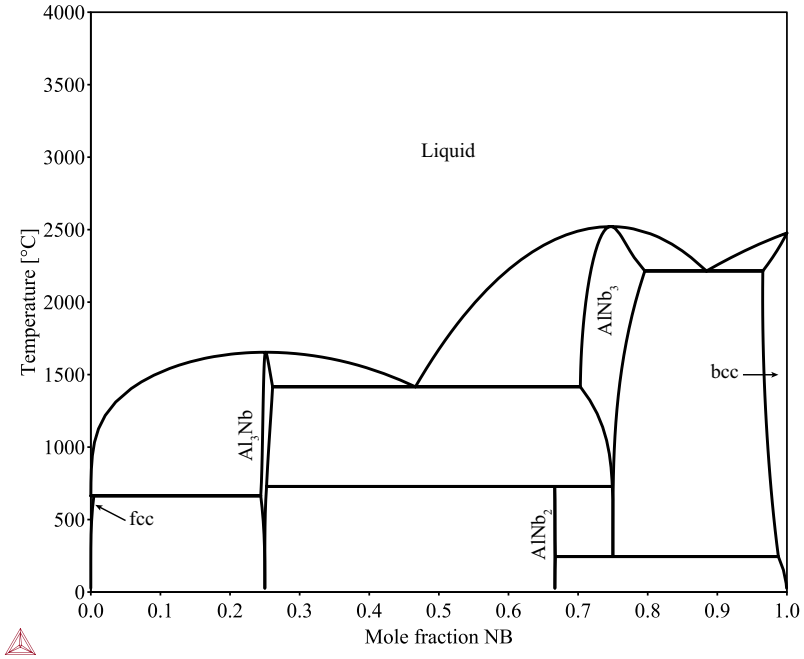

Figure 7. Phase diagram of the Al-Nb binary system with liquid interaction parameters from Witusiewicz et al. [11].

$NbNi_8$ is slightly above the convex hull. According to literature [53–55], the formation of $NbNi_8$ requires a long annealing time and numerous excess vacancies from either rapid quenching or charged-particle irradiation. Therefore, $NbNi_8$ might be stabilized by vacancy mechanism. Because the DFT calculation of $NbNi_8$ does not contain any vacancy, the $NbNi_8$ is not sufficiently stable to form the convex hull in the Nb-Ni binary system. Table 1 shows the enthalpy of formation of compounds obtained from the published thermodynamic database [15] in parenthesis. The two stable intermediate compounds are Nb_7Ni_6 and $NbNi_3$, which agree with published experimental phase diagram [57] and assessed thermodynamic database [13]. Other end-member energies are all above the convex hull. To evaluate the interaction parameters between end-members, the correspond SQSs are generated. Table 5 lists the calculated mixing energy from $(Nb_{0.5}Ni_{0.5})Ni_3$ and $Nb(Nb_{0.5}Ni_{0.5})_3$ SQS. The $Nb_7(Nb_{0.5}Ni_{0.5})_6$ SQS is generated but the convergent problem occurs during the DFT calculations. Thus, the mixing energy of Nb_7Ni_6 SQS is unavailable.

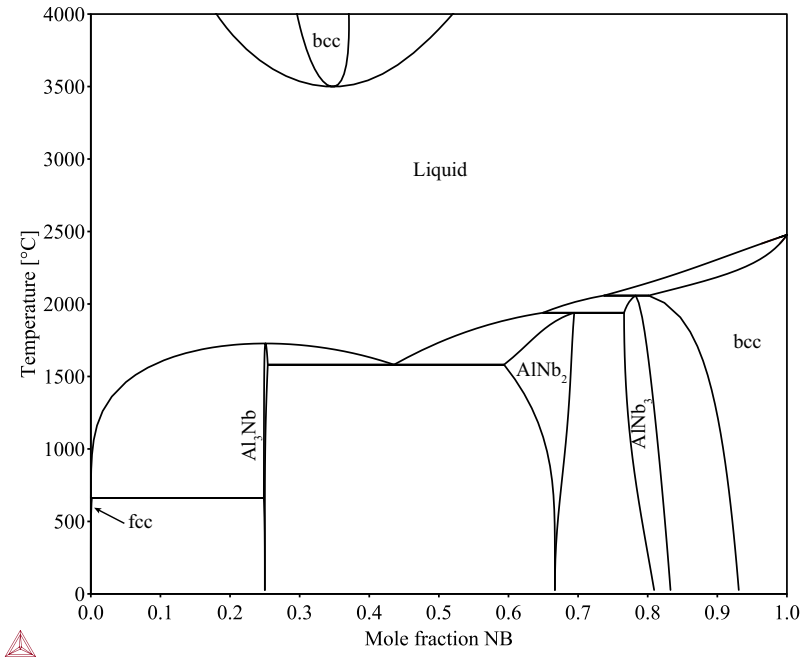

Figure 8. CALPHAD assessed phase diagram of the Al-Nb binary system from He et al. [12].

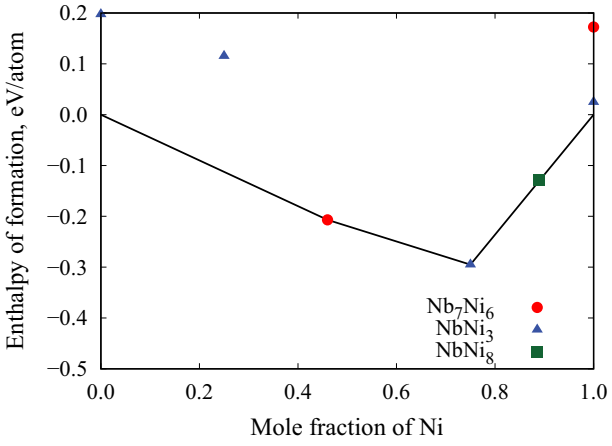

Figure 9. Formation enthalpy for binary compounds and their corresponding end-members of sublattice model, (Nb,Ni)(Nb, Ni)$_3$ and Nb$_7$(Nb,Ni)$_6$, with connected convex hull of the Nb-Ni binary system.

Similar to the Al-Nb binary system, only the temperature independent interaction parameters are evaluated and listed in Table 7.

Figure 10 shows the calculated enthalpy of mixing across the composition range for fcc-, bcc-, and hcp-disordered structures. For fcc results, it seems that the data at 75 and 87.5 at.% Nb are outlier because they are more stable than other data points. For hcp results, similar to fcc, the data at 50 at.% Nb are more stable than the nearest data points. Applying the same analysis for SQS in the Al-Nb section, we will exclude the outlier data points from the further evaluations. For bcc results, the data at 12.5, 25, 37.5, and 50 at.% Nb are considered outlier. Because the ground state structure of Nb is bcc, the data point at higher at.% Nb can be considered more reliable. The data at 12.5, 25, 37.5, and 50 at.% Nb will be excluded. Figure 11 shows finite temperature mixing energy of fcc SQS at 0, 500, 1000, 1500 and 2000 K. Assuming regular mixing behavior, the bcc-disordered interaction parameter was obtained using only the 75 at.% Nb datasets. The interaction parameters of fcc- and hcp-disordered phases can be obtained from the same procedure and are listed in Table 6.

By employing the ideal solution for the liquid phase, the Nb-Ni phase diagram with the first-principles calculations data is plotted in Figure 12. Both Nb$_7$Ni$_6$ and NbNi$_3$ phases are stable while NbNi$_8$ is unstable. NbNi$_3$ stability extends to a high temperature before decompose into hcp-disordered and liquid phase through the peritectic reaction. The hcp-disordered phase is presented at high temperature but is not presented in any published phase diagrams [13–15,57–59]. Figure 13 shows the calculated phase diagram from published thermodynamic database from Chen et al. [15] that have the NbNi$_8$ phase stable up to 515 °C. The solubility of Ni-rich fcc-disordered phase seems to be narrower compared to published phase diagram. This might be the consequence from the vibrational contribution to the free energy of the reference phases. In case of fcc Nb, imaginary phonon frequencies have appear. This results in error when performing the

Table 7. CALPHAD parameters for the Al-Nb-Ni thermodynamic database (part 2).

Phases	Gibbs/Interactions	Parameters
$AlNb_3$	${}^{0}G^{AlNb_3}_{Al_4}$	$4\ {}^{a0}G^{fcc}_{Al}$ +30453 - 24.17T
	${}^{0}G^{AlNb_3}_{AlNb_3}$	${}^{a0}G^{fcc}_{Al}$ +3 ${}^{a0}G^{bcc}_{Nb}$ − 69820 - 16.78T
	${}^{0}G^{AlNb_3}_{AlNi_3}$	${}^{a0}G^{fcc}_{Al}$ +3 ${}^{a0}G^{fcc}_{Ni}$ − 103361 - 0.72T
	${}^{0}G^{AlNb_3}_{NbAl_3}$	$3\ {}^{a0}G^{fcc}_{Al}$ + ${}^{a0}G^{bcc}_{Nb}$ − 25564 + 8.49T
	${}^{0}G^{AlNb_3}_{Nb_4}$	$4\ {}^{a0}G^{bcc}_{Nb}$ +40578 - 8.88T
	${}^{0}G^{AlNb_3}_{NbNi_3}$	${}^{a0}G^{bcc}_{Nb}$ +3 ${}^{a0}G^{fcc}_{Ni}$ − 85851 - 17.32T
	${}^{0}G^{AlNb_3}_{NiAl_3}$	$3\ {}^{a0}G^{fcc}_{Al}$ + ${}^{a0}G^{fcc}_{Ni}$ − 92574 - 20.18T
	${}^{0}G^{AlNb_3}_{NiNb_3}$	$3\ {}^{a0}G^{bcc}_{Nb}$ + ${}^{a0}G^{fcc}_{Ni}$ − 21320 - 4.38T
	${}^{0}G^{AlNb_3}_{Ni_4}$	$4\ {}^{a0}G^{fcc}_{Ni}$ +52889 - 27.85T
	${}^{0}L^{AlNb_3}_{Al,Nb:Nb}$	+20000
Al_3Ni-$D0_{11}$	${}^{0}G^{Al_3Ni}_{Al_{12}Ni_4}$	$16\ {}^{a0}G^{fcc}_{Al}$ − 620774 + 19.91T + 4.67×10^{-2}T^2
Al_3Ni_2-$D5_{13}$	${}^{0}G^{Al_{0.6}Ni_{0.4}}_{Al}$	${}^{a0}G^{fcc}_{Al}$ +17122 - 3.50T + 2.19×10^{-3}T^2
	${}^{0}G^{Al_{0.6}Ni_{0.4}}_{Al_{0.6}Ni_{0.4}}$	$0.6\ {}^{a0}G^{fcc}_{Al}$ +0.4 ${}^{a0}G^{fcc}_{Ni}$ − 58466 + 2.23T + 3.15×10^{-3}T^2
	${}^{0}G^{Al_{0.6}Ni_{0.4}}_{Ni_{0.6}Al_{0.4}}$	$0.4\ {}^{a0}G^{fcc}_{Al}$ +0.6 ${}^{a0}G^{fcc}_{Al}$ − 28881 - 1.44T + 2.31×10^{-3}T^2
	${}^{0}G^{Al_{0.6}Ni_{0.4}}_{Ni}$	${}^{a0}G^{fcc}_{Ni}$ +31967 - 3.86T − 1.08×10^{-4}T^2
	${}^{0}L\,{}^{0}L^{Al_{0.6}Ni_{0.4}}_{Al,Ni:Al}$	− 10388 + 1.02T + 2.08×10^{-4}T^2
	${}^{0}L^{Al_{0.6}Ni_{0.4}}_{Al:Al,Ni}$	− 16305 + 1.17T + 3.77×10^{-4}T^2
	${}^{0}L^{Al_{0.6}Ni_{0.4}}_{Al,Ni:Ni}$	− 10388 + 1.02T + 2.08×10^{-4}T^2
	${}^{0}L^{Al_{0.6}Ni_{0.4}}_{Ni:Al,Ni}$	− 16305 + 1.17T + 3.77×10^{-4}T^2
Al_4Ni_3	${}^{0}G^{Al_4Ni_3}_{Al_4Ni_3}$	$4\ {}^{a0}GAl^{fcc}$ +3 ${}^{a0}G^{fcc}_{Ni}$ − 418712 + 9.04T + 2.24×10^{-2}T^2
Al_3Ni_5	${}^{0}G^{Al_3Ni_5}_{Al_3Ni_5}$	$3\ {}^{a0}G^{fcc}_{Al}$ +5 ${}^{a0}G^{fcc}_{Ni}$ − 432983 + 8.15T + 1.49×10^{-2}T^2
6*Nb_7Ni_6	${}^{0}G^{Nb_7Ni_6}_{Al_{13}}$	$13\ {}^{a0}G^{fcc}_{Al}$ +134471 - 67.40T
	${}^{0}G^{Nb_7Ni_6}_{Al_7Nb_6}$	$7\ {}^{a0}G^{fcc}_{Al}$ +6 ${}^{a0}G^{bcc}_{Nb}$ +33138 - 22.23T
	${}^{0}G^{Nb_7Ni_6}_{Al_7Ni_6}$	$7\ {}^{a0}G^{fcc}_{Al}$ +6 ${}^{a0}G^{fcc}_{Ni}$ − 594334 - 4.11T
	${}^{0}G^{Nb_7Ni_6}_{Nb_7Al_6}$	$6\ {}^{a0}G^{fcc}_{Al}$ +7 ${}^{a0}G^{bcc}_{Nb}$ − 312429 + 49.76T
	${}^{0}G^{Nb_7Ni_6}_{Nb_{13}}$	$13\ {}^{a0}G^{bcc}_{Nb}$ +216308 + 11.64T
	${}^{0}G^{Nb_7Ni_6}_{Nb_7Ni_6}$	$7\ {}^{a0}G^{bcc}_{Nb}$ +6 ${}^{a0}G^{fcc}_{Ni}$ − 259502 + 6.46T
$NbNi_3$	${}^{0}G^{NbNi_3}_{Al_4}$	$4\ {}^{a0}G^{fcc}_{Al}$ +12688
	${}^{0}G^{NbNi_3}_{AlNb_3}$	${}^{a0}G^{fcc}_{Al}$ +3 ${}^{a0}G^{bcc}_{Nb}$ − 39713 + 12.30T
	${}^{0}G^{NbNi_3}_{AlNi_3}$	${}^{a0}G^{fcc}_{Al}$ +3 ${}^{a0}G^{fcc}_{Ni}$ − 158086 + 10.6T
	${}^{0}G^{NbNi_3}_{NbAl_3}$	$3\ {}^{a0}G^{fcc}_{Al}$ + ${}^{a0}G^{bcc}_{Nb}$ − 128407 + 24.70
	${}^{0}G^{NbNi_3}_{Nb_4}$	$4\ {}^{a0}G^{bcc}_{Nb}$ +76149 - 2.21T
	${}^{0}G^{NbNi_3}_{NbNi_3}$	${}^{a0}G^{bcc}_{Nb}$ +3 ${}^{a0}G^{fcc}_{Ni}$ − 113880 + 2.12T
	${}^{0}G^{NbNi_3}_{NiAl_3}$	$3\ {}^{a0}G^{fcc}_{Al}$ + ${}^{a0}G^{fcc}_{Ni}$ − 99228 - 0.82T
	${}^{0}G^{NbNi_3}_{NiNb_3}$	$3\ {}^{a0}G^{bcc}_{Nb}$ + ${}^{a0}G^{fcc}_{Ni}$ +44509 - 16.48T
	${}^{0}G^{NbNi_3}_{Ni_4}$	$4\ {}^{a0}G^{fcc}_{Ni}$ +9539 - 3.63T
	${}^{0}L^{NbNi_3}_{Nb,Ni:Ni}$	+8000
bcc-B2	${}^{0}G^{bcc-B2}_{Al_2}$	$2\ {}^{a0}G^{fcc}_{Al}$ +18500 - 3.94T
	${}^{0}G^{bcc-B2}_{AlNb}$	${}^{a0}G^{fcc}_{Al}$ + ${}^{a0}G^{bcc}_{Nb}$ − 6774 + 6.18T
	${}^{0}G^{bcc-B2}_{AlNi}$	${}^{a0}G^{fcc}_{Al}$ + ${}^{a0}G^{fcc}_{Ni}$ − 127901 + 2.60T
	${}^{0}G^{bcc-B2}_{NbAl}$	${}^{a0}G^{fcc}_{Al}$ + ${}^{a0}G^{bcc}_{Nb}$ − 6774 + 6.18T
	${}^{0}G^{bcc-B2}_{Nb_2}$	$2\ {}^{a0}G^{bcc}_{Nb}$ +1000 + T
	${}^{0}G^{bcc-B2}_{NbNi}$	${}^{a0}G^{bcc}_{Nb}$ + ${}^{a0}G^{fcc}_{Ni}$ − 3492 - 14.01T
	${}^{0}G^{bcc-B2}_{NiAl}$	${}^{a0}G^{fcc}_{Al}$ + ${}^{a0}G^{fcc}_{Ni}$ − 127901 + 2.60T
	${}^{0}G^{bcc-B2}_{NiNb}$	${}^{a0}G^{bcc}_{Nb}$ + ${}^{a0}G^{fcc}_{Ni}$ − 3492 - 14.01T
	${}^{0}G^{bcc-B2}_{Ni_2}$	$2\ {}^{a0}G^{fcc}_{Ni}$ +18203 - 8.01T
	${}^{0}L^{bcc-B2}_{Ni:Al,Ni}$	− 60000 - 4T
	${}^{0}L^{bcc-B2}_{Al,Ni:Ni}$	− 60000 - 4T

[a]SGTE pure elements database[19].

integration for vibrational energy owing to the ignoring of the imaginary frequencies. This results in the inaccuracy on the finite temperature part of the interaction parameter of the disordered phases. The parameters for the Nb-Ni binary system are listed in Table 7. Using the liquid interaction from Matsumoto et al. [60], the Nb-Ni phase diagram is shown in Figure 14. With liquid interaction parameters, the stability of high temperature hcp-disordered phase is suppressed. The stability of both Nb_7Ni_6 and $NbNi_3$ phases are similar to that appearing in the published phase diagram [15]. The solubility of Nb_7Ni_6 is slightly smaller. This probably resulted from the lack of interaction

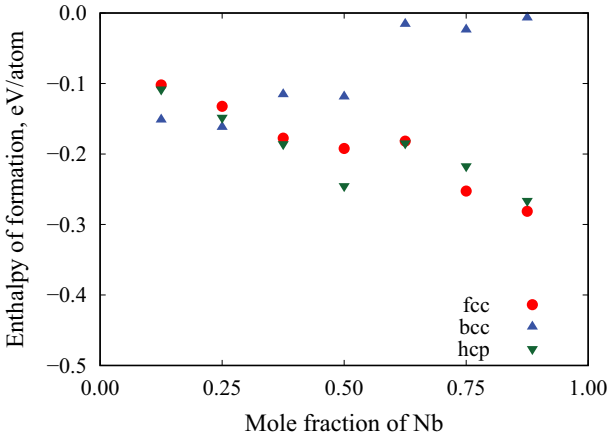

Figure 10. Mixing enthalpy of fcc-, bcc-, and hcp-disordered phases from SQS for the Nb-Ni binary system.

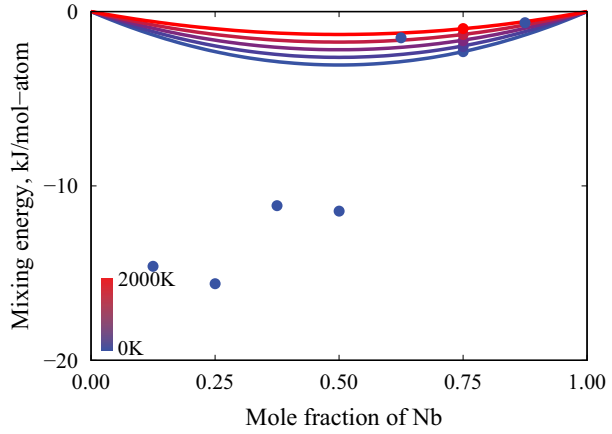

Figure 11. Finite temperature mixing energy of the Nb-Ni bcc-disordered SQS (point) with CALPHAD excess energy from fitted interaction parameters using the mixing energy (line).

parameters. The solid solubility of $NbNi_3$ is much larger compared to the published phase diagram. The lack of the temperature dependent term in the interaction parameters and the error in the fcc-disordered energy might be the causes for larger solubility range. The bcc-disordered phase boundary is comparable to the published phase diagram.

3.4. Al-Nb-Ni

The thermodynamic database for the Al-Nb-Ni ternary system is established by combining the Al-Ni, Al-Nb, and Nb-Ni binary systems together. All the stable ternary compounds listed in Materials Project database [40] and indicated in experimental data [16,61], including intermediate ternary compounds and extended solid solution from binary, are added to database. There are only two intermediate ternary phases presented ($AlNbNi_2$ and AlNbNi). Another ternary phase (M phase) that has been identified as high temperature phase by Du et al. [16,62–64]. It has the structure that similar to μ-Nb_7Ni_6 with higher Al content. Owing to the complexity of the M phase structure, it will be excluded from the modeling. Based on the experimental investigation [16,61], there are limited solubility range for $AlNbNi_2$ ternary phase. Thus, to simplify the model, stoichiometric description will be used for $AlNbNi_2$. AlNbNi phase has small solubility range for Nb but large solubility between Al and Ni. The (Al,Ni)Nb (Al,Ni) sublattice will be used to represent the solubility of Al and Ni elements in AlNbNi phase. Table 4 lists all the ternary sublattice models used in the Al-Nb-Ni system. Table 1

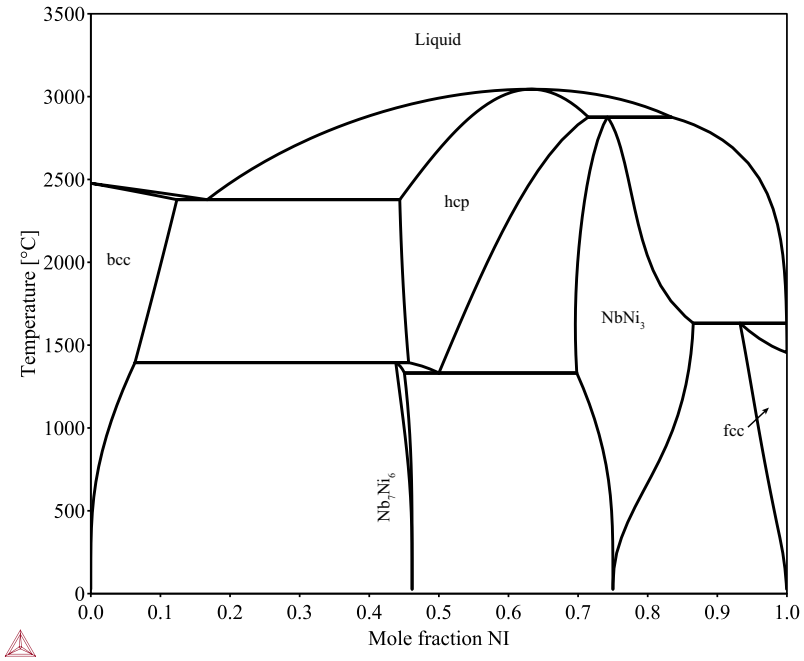

Figure 12. Phase diagram of the Nb-Ni binary system with ideal liquid model.

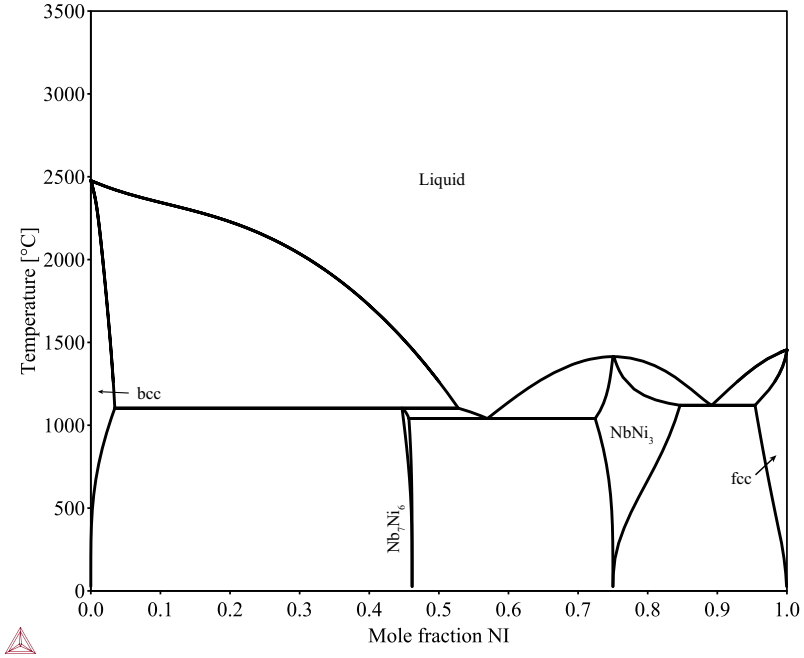

Figure 13. Phase diagram of the Nb-Ni binary system with liquid interaction parameters from Matsumoto et al. [60].

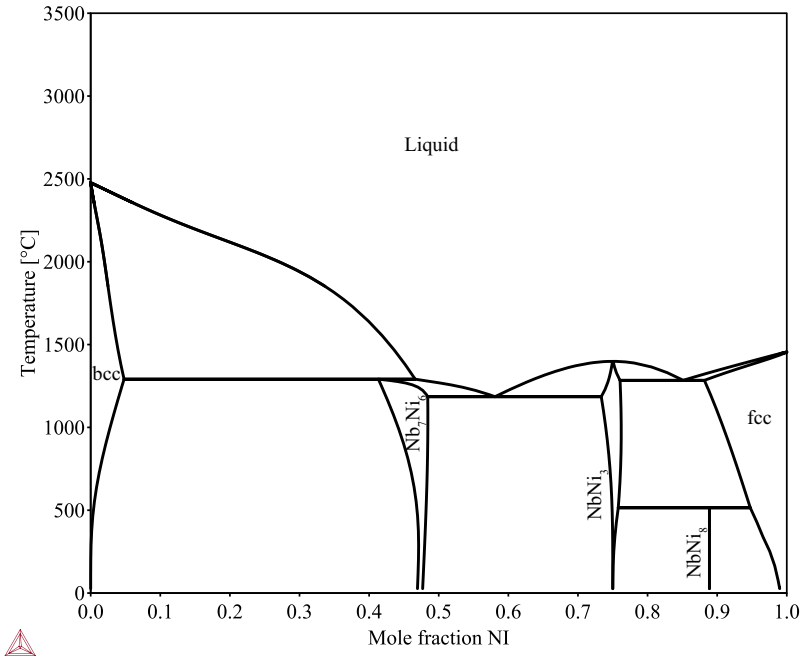

Figure 14. CALPHAD assessed phase diagram of the Nb-Ni binary system from Chen et al. [15].

presents formation enthalpy and entropy for all ternary compounds and the end-members of the sublattice models. Additional mixing enthalpy from SQS for ternary $((Al_{0.5}Ni_{0.5})NbNi$, $AlNb(Al_{0.5}Ni_{0.5})$, and $(Al_{0.5}Ni_{0.5})Nb(Al_{0.5}Ni_{0.5}))$ and extended solubility phases from binary are listed in Table 5. Similar to the binary interaction parameter evaluations, the SQS mixing energy of corresponding each sublattice model were used. As aforementioned, only 0 K mixing energy calculations are performed owing to the high computational cost for the finite temperature properties of the SQS. Owing to the unavailable of the first-principles liquid data, only binary liquid interaction parameters from the binaries are included. The ternary liquid

Table 8. CALPHAD parameters for the Al-Nb-Ni thermodynamic database (part 3).

Phases	Gibbs/Interactions	Parameters
fcc-$L1_2$	${}^{0}G^{fcc-L1_2}_{Al_4}$	$4\ {}^{a0}G^{fcc}_{Al}$
	${}^{0}G^{fcc-L1_2}_{AlNb_3}$	${}^{a0}G^{fcc}_{Al}$ +3 ${}^{a0}G^{bcc}_{Nb}$ − 44216 + 6.01T
	${}^{0}G^{fcc-L1_2}_{AlNi_3}$	3 ${}^{a0}G^{fcc}_{Al}$ + ${}^{a0}G^{fcc}_{Ni}$ − 167212 + 3.67T
	${}^{0}G^{fcc-L1_2}_{NbAl_3}$	3 ${}^{a0}G^{fcc}_{Al}$ + ${}^{a0}G^{bcc}_{Nb}$ − 102105 + 10.21T
	${}^{0}G^{fcc-L1_2}_{Nb_4}$	$4\ {}^{a0}G^{fcc}_{Nb}$
	${}^{0}G^{fcc-L1_2}_{NbNi_3}$	${}^{a0}G^{bcc}_{Nb}$ +3 ${}^{a0}G^{fcc}_{Ni}$ − 51723 - 13.76T
	${}^{0}G^{fcc-L1_2}_{NiAl_3}$	3 ${}^{a0}G^{fcc}_{Al}$ + ${}^{a0}G^{fcc}_{Ni}$ − 83972 - 10.80T
	${}^{0}G^{fcc-L1_2}_{NiNb_3}$	3 ${}^{a0}G^{bcc}_{Nb}$ + ${}^{a0}G^{fcc}_{Ni}$ +39720 + 10.21T
	${}^{0}G^{fcc-L1_2}_{Ni_4}$	$4\ {}^{a0}G^{fcc}_{Ni}$
	${}^{0}L^{fcc-L1_2}_{Al,Nb:Ni}$	− 50000
	${}^{0}L^{fcc-L1_2}_{Al,Ni:Ni}$	+20000
$AlNbNi_2$	${}^{0}G^{AlNbNi_2}_{AlNbNi_2}$	${}^{a0}G^{fcc}_{Al}$ + ${}^{a0}G^{bcc}_{Nb}$ +2 ${}^{a0}G^{fcc}_{Ni}$ − 168240 - 16T
AlNbNi	${}^{0}G^{AlNbNi}_{AlNbAl}$	2 ${}^{a0}G^{fcc}_{Al}$ + ${}^{a0}G^{bcc}_{Nb}$ − 84747 + 14.40T
	${}^{0}G^{AlNbNi}_{AlNbNi}$	${}^{a0}G^{fcc}_{Al}$ + ${}^{a0}G^{bcc}_{Nb}$ + ${}^{a0}G^{fcc}_{Ni}$ − 124500 + 9.66T
	${}^{0}G^{AlNbNi}_{NiNbAl}$	${}^{a0}G^{fcc}_{Al}$ + ${}^{a0}G^{bcc}_{Nb}$ + ${}^{a0}G^{fcc}_{Ni}$ − 115641 + 8.64T
	${}^{0}G^{AlNbNi}_{NiNbNi}$	${}^{a0}G^{bcc}_{Nb}$ 2 ${}^{a0}G^{fcc}_{Ni}$ − 56280 + 3T
	${}^{0}L^{AlNbNi}_{Al,Ni:Nb:Ni}$	− 31000
	${}^{0}L^{AlNbNi}_{Al:Nb:Al,Ni}$	− 110000

[a] SGTE pure elements database[19].

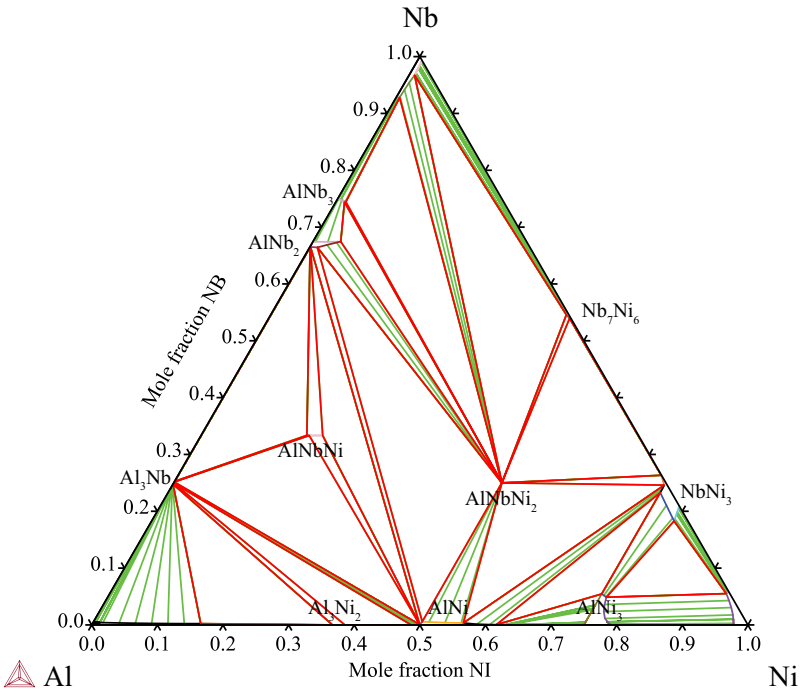

Figure 15. Isothermal section of the Al-Nb-Ni phase diagram at 900 °C.

interaction parameters are all zero. Tables 6, 7 , and 8 list the available parameters of the Al-Nb-Ni ternary system.

Figure 15 shows the isothermal section at 900 °C of the Al-Nb-Ni ternary system. Two ternary intermediate compounds ($AlNbNi_2$ and AlNbNi) are stable at this temperature, which agrees with the published ternary phase diagram from Bhedwar et al. [61] and the assessed thermodynamic database from Du et al. [16]. The extended solubility from the binary are presented in $AlNb_3$, $AlNb_2$, AlNi-B2, $AlNi_3$, Nb_7Ni_6, and $NbNi_3$ phases. The solubility range of AlNbNi phase is limited (<5%) comparing to the phase diagrams from Bhedwar et al. [61] and Du et al. [16] (>50%). The absence of finite temperature interaction parameter might contribute to the narrower solubility range of the AlNbNi phase. It is proved that the Al-Nb-Ni thermodynamic database from the first-principles data can correctly reproduce the published phase diagram. Figure 16 shows the isothermal section at 1127 °C. As the temperature increases, the liquid phase field become larger and all the extended solubility from binary compounds seem to become larger

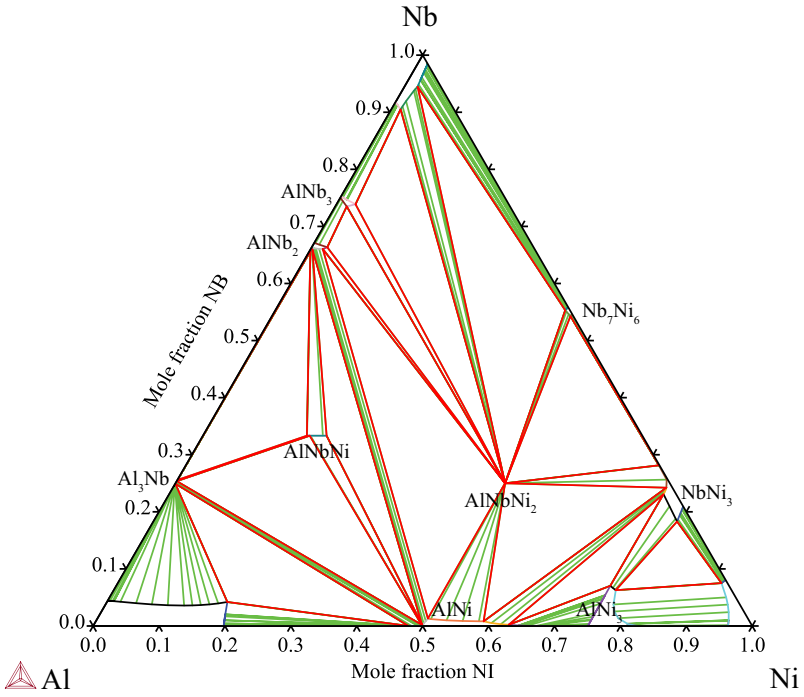

Figure 16. Isothermal section of the Al-Nb-Ni phase diagram at 1127 °C.

as well. Based on the literature, M phase is presented at this temperature. Owing to the exclusion of the M phase from the modeling, the calculated phase diagram cannot accurately reproduce the phase diagram in the region where M phase is presented. However, in other regions, the first-principles phase diagram is similar to the published phase diagram [16,61].

4. Conclusion

In this work, we demonstrate that, by employing only the data from first-principles calculations, the thermodynamic database for the Al-Nb-Ni ternary system can be correctly and rapidly constructed. All the invariant reactions can be successfully reproduced. Although, it cannot accurately reproduce the solubility limit and transformation temperatures of every phases, it helps by rapidly establishing a preliminary thermodynamic databases. To achieve more accurate prediction of the calculated phase diagram, higher approximations for vibrational contribution, such as quasi-harmonic or even anharmonic approximations might be required. Other contributions to the free energy, such as magnetic ordering should be considered. Traditional CALPHAD thermodynamic assessment requires several experimental data, which are costly and time consuming. By integrating the DFT calculations data, which will help accelerate the thermodynamic database development, it provides a guidance on which additional data point need to further improve the accuracy of the database. By using along side with the uncertainty quantification (UQ) [65], the area of phase diagram that need more accurate experimental or DFT calculations data point can be identified. The semi-automated or automated generation of thermodynamic database for many unknown systems can be achieved. As previously mention, the sublattice models for both σ and μ phases are simplified in order to reduce the complexity of the first-principles calculations. To enable the higher compatibility with other thermodynamic databases, the modification of the sublattice models might needed. However, it is possible to directly replace the sublattice model of both phases in the future work without any re-optimization of the parameters in the thermodynamic database. The main challenge for rapid development of the first-principles thermodynamic database is the free energy description of the liquid phase. It is possible to calculate the free energy of liquid phase from DFT; however, it is rather computational expensive owing to the nature of the liquid phase that usually require anharmonic contribution because it existed at high temperature near or above melting point [66]. Currently, performing experimental measurement of the temperature and compositions upon the melting of the liquid phase are simpler and faster than using first-principles calculations. Therefore, experimental data point is critical in achieving highly accurate thermodynamic assessment for any system. First-principles calculations play an important role on reducing the number of required experimental data points and help saving time and cost for the multi-component thermodynamic database development.

Acknowledgements

The authors gratefully acknowledge Numerical Materials Simulator supercomputing resources from the Research Network and Facility Services Division (RNFS), National Institute for Materials Science (NIMS), Japan. We would like to thank Editage (www.editage.com) for English language editing.

Disclosure statement

No potential conflict of interest was reported by the author(s).

Funding

This work was supported by Council for Science, Technology and Innovation(CSTI), Cross-ministerial Strategic Innovation Promotion Program (SIP), "Materials Integration for revolutionary design system of structural materials", and the Grants-in-Aid for Scientific Research (KAKENHI) grant number [21H01607].Funding agency: Japan Science and Technology Agency (JST) and Japan Society for the Promotion of Science (JSPS).

ORCID

Arkapol Saengdeejing https://orcid.org/0000-0001-8739-3262
Ryoji Sahara https://orcid.org/0000-0003-0788-2985
Yoshiaki Toda https://orcid.org/0000-0002-8343-2890

Data availability statement

The raw data required to reproduce these findings cannot be shared at this time because they are being used on an ongoing study. The process data required to reproduce the original phase diagram calculations is available in the tdb file upon request.

References

[1] Ohtani H. The CALPHAD method. In: Czichos H, Saito T Smith L, editors. Springer handbook of materials measurement methods. Berlin, Heidelberg: Springer Berlin Heidelberg; 2006. p. 1001–1030.
[2] Ansara I, Dupin N, Lukas HL, et al. Thermodynamic assessment of the Al-Ni system. J Alloys Compd. 1997;247(1–2):20–30. doi: 10.1016/S0925-8388(96)02652-7
[3] Dupin N, Ansara I, Sundman B. Thermodynamic re-assessment of the ternary system Al-Cr-Ni. CALPHAD. 2001;25(2):279–298. doi: 10.1016/S0364-5916(01)00049-9
[4] Witusiewicz V, Bondar A, Hecht U, et al. The Al–B–Nb–Ni system: III. thermodynamic re-evaluation of the constituent binary system Al–ti. J Alloys Compd. 2008;465(1):64–77. doi: 10.1016/j.jallcom.2007.10.061
[5] De Keyzer J, Cacciamani G, Dupin N, et al. Thermodynamic modeling and optimization of the Fe–Ni–Ti system. CALPHAD. 2009;33(1):109–123. Experimental and Computational investigation of intermetallic systems: A Special Issue Dedicated to Prof. Riccardo Ferro. doi:10.1016/j.calphad.2008.10.003
[6] Zhu W, Duarte L, Leinenbach C. Experimental study and thermodynamic assessment of the Cu–Ni–Ti system. CALPHAD. 2014;47:9–22. doi: 10.1016/j.calphad.2014.06.002
[7] Saengdeejing A, Saal JE, Manga VR, et al. Defects in boron carbide: first-principles calculations and calphad modeling. Acta Mater. 2012 12;60(20):7207–7215. doi: 10.1016/j.actamat.2012.09.029
[8] Davey T, Tran ND, Saengdeejing A, et al. First-principles-only calphad phase diagram of the solid aluminium-nickel (Al-Ni) system. CALPHAD. 2020;71:102008. doi: 10.1016/j.calphad.2020.102008
[9] Saengdeejing A, Sahara R, Toda Y. Al–Ni–Ti thermodynamic database from first-principles calculations. CALPHAD. 2024 Mar;84:102658. doi: 10.1016/j.calphad.2023.102658
[10] Jorda J, Flükiger R, Muller J. A new metallurgical investigation of the niobium-aluminium system. J Less-Common Met. 1980;75(2):227–239. doi: 10.1016/0022-5088(80)90120-4
[11] Witusiewicz V, Bondar A, Hecht U, et al. The Al–B–Nb–Ti system. J Alloys Compd. 2009 Mar;472(1–-2):133–161. doi: 10.1016/j.jallcom.2008.05.008
[12] He C, Stein F, Palm M. Thermodynamic description of the systems Co–Nb, Al–Nb and Co–Al–Nb. J Alloys Compd. 2015 Jul;637:361–375. doi: 10.1016/j.jallcom.2015.02.182
[13] Bolcavage A, Kattner UR. A reassessment of the calculated Ni-Nb phase diagram. J Phase Equilib. 1996 Apr;17(2):92–100. doi: 10.1007/BF02665782
[14] Joubert JM, Sundman B, Dupin N. Assessment of the niobium–nickel system. CALPHAD. 2004 Sep;28(3):299–306. doi: 10.1016/j.calphad.2004.09.004
[15] Chen H, Du Y. Refinement of the thermodynamic modeling of the Nb–Ni system. CALPHAD. 2006 Sep;30(3):308–315. doi: 10.1016/j.calphad.2006.02.005
[16] Du Y, Chang Y, Gong W, et al. Thermodynamic properties of the Al–Nb–Ni system. Intermetallics. 2003;11(10):995–1013. doi: 10.1016/S0966-9795(03)00123-7
[17] Liu ZK. First-principles calculations and CALPHAD modeling of thermodynamics. J Phase Equilib Diffus. 2009 sep;30(5):517–534. doi: 10.1007/s11669-009-9570-6
[18] Bragg WL, Williams EJ. The effect of thermal agitation on atomic arrangement in alloys. Proc R Soc Lond, Ser A. 1934 Jul;145(855):699–730.
[19] Dinsdale A. SGTE data for pure elements. CALPHAD. 1991;15(4):317–425. doi: 10.1016/0364-5916(91)90030-N
[20] Redlich O, Kister AT. Algebraic representation of thermodynamic properties and the classification of solutions. Ind Eng Chem. 1948;40(2):345–348. doi: 10.1021/ie50458a036
[21] Lukas H, Fries SG, Sundman B. Computational thermodynamics. Cambridge: Cambridge University Press; 2007.
[22] Hillert M. The compound energy formalism. J Alloys Compd. 2001;320(2):161–176. doi: 10.1016/S0925-8388(00)01481-X
[23] Kubaschewski O. Metallurgical thermochemistry. Int Ser Mater Sci Technol. 1977;24:478.
[24] Andersson JO, Helander T, Höglund L, et al. Thermo-calc & dictra, computational tools for materials science. CALPHAD. 2002;26(2):273–312. doi: 10.1016/S0364-5916(02)00037-8
[25] Kresse G, Joubert D. From ultrasoft pseudopotentials to the projector augmented-wave method. Phys Rev B. 1999;59(3):1758. doi: 10.1103/PhysRevB.59.1758

[26] Kresse G. Efficient iterative schemes for ab initio total-energy calculations using a plane-wave basis set. Phys Rev B. 1996 Oct;54(16):11169–11186. doi: 10.1103/PhysRevB.54.11169
[27] Blóchl PE. Projector augmented-wave method. Phys Rev B. 1994;50(24):17953–17979. doi: 10.1103/PhysRevB.50.17953
[28] Perdew JP, Burke K, Ernzerhof M. Generalized gradient approximation made simple. Phys Rev Lett. 1996 Oct;77(18):3865–3868. doi: 10.1103/PhysRevLett.77.3865
[29] Monkhorst HJ, Pack JD. Special points for brillouin-zone integrations. Phys Rev B. 1976 Jun;13(12):5188–5192. doi: 10.1103/PhysRevB.13.5188
[30] Methfessel M, Paxton AT. High-precision sampling for brillouin-zone integration in metals. Phys Rev B. 1989;40(6):3616–3621. doi: 10.1103/PhysRevB.40.3616
[31] Blóchl PE, Jepsen O, Andersen OK. Improved tetrahedron method for brillouin-zone integrations. Phys Rev B. 1994;49(23):16223–16233. doi: 10.1103/PhysRevB.49.16223
[32] Landau L, Lifshitz E. Statistical physics. Oxford: Pergamon Press; 1980.
[33] van de Walle A, Asta M, Ceder G. The alloy theoretic automated toolkit: a user guide. CALPHAD. 2002 Dec;26(4):539–553. doi: 10.1016/S0364-5916(02)80006-2
[34] Shang S, Wang Y, Liu ZK. First-principles calculations of phonon and thermodynamic properties in the boron-alkaline earth metal binary systems: B-Ca, B-Sr, and B-Ba. Phys Rev B. 2007 jan;75(2):1–11. doi: 10.1103/PhysRevB.75.024302
[35] Zunger A, Wei SH, Ferreira LG, et al. Special quasirandom structures. Phys Rev Lett. 1990 Jul;65(3):353–356. doi: 10.1103/PhysRevLett.65.353
[36] Sanchez JM. Cluster expansion and the configurational theory of alloys. Phys Rev B. 2010 Jun;81(22):224202. doi: 10.1103/PhysRevB.81.224202
[37] Wolverton C. Crystal structure and stability of complex precipitate phases in Al–Cu– Mg–(Si) and Al–Zn–Mg alloys. Acta Mater. 2001;49(16):3129–3142. doi: 10.1016/S1359-6454(01)00229-4
[38] Jiang C, Wolverton C, Sofo J, et al. First-principles study of binary bcc alloys using special quasirandom structures. Phys Rev B. 2004 Jun;69(21):214202. doi: 10.1103/PhysRevB.69.214202
[39] Shin D, Arróyave R, Liu ZK, et al. Thermodynamic properties of binary hcp solution phases from special quasirandom structures. Phys Rev B. 2006 Jul;74(2):024204. doi: 10.1103/PhysRevB.74.024204
[40] Jain A, Ong SP, Hautier G, et al. Commentary: the materials project: a materials genome approach to accelerating materials innovation. APL Mater. 2013;1(1):011002. doi: 10.1063/1.4812323
[41] Maas J, Bastin G, van Loo F, et al. The texture in diffusion-grown layers of trialuminides MeAl3 (Me=Ti, V, Ta, Nb, Zr, Hf) and VNi3. Z Metallkd. 1983;74(5):294–299. doi: 10.1515/ijmr-1983-740506
[42] Shamrai V. The volume dependence of T_c of ternary A-15 phases. J Low Temp Phys. 1984 Jul;56(1):51–67. doi: 10.1007/BF00681455
[43] Fang T, Kennedy SJ, Quan L, et al. The structure and paramagnetism of Ni_3Nb. J Phys: Condens Matter. 1992 mar;4(10):2405. doi: 10.1088/0953-8984/4/10/007
[44] Rossteutscher W, Schubert K. Constitution of vanadium zinc alloy system. Z Metallkd. 1964;55(10):617–618. doi: 10.1515/ijmr-1964-551013
[45] Waki S, Yamaguchi Y, Mitsugi K. Superconductivity of Ni_2NbX (X=Al, Ga and Sn). J Phys Soc Jpn. 1985;54(5):1673–1676. doi: 10.1143/JPSJ.54.1673
[46] Raman A, Schubert K. Über den aufbau einiger zu $TiAl_3$ verwandter legierungsreihen iii. untersuchungen in einigen Ti-Ni-Al- und Ti-Cu-Al-systemen. Z Metallkd. 1965;56(2):99–104. doi: 10.1515/ijmr-1965-560207
[47] Shilo I, Franzen HF, Schiffman RA. Enthalpies of formation of niobium aluminides as determined by the knudsen effusion method. J Electrochem Soc. 1982 Jul;129(7):1608–1613. doi: 10.1149/1.2124218
[48] Meschel S, Kleppa O. Standard enthalpies of formation of 4d aluminides by direct synthesis calorimetry. J Alloys Compd. 1993 Jan;191(1):111–116. doi: 10.1016/0925-8388(93)90280-Z
[49] Mahdouk K, Gachon JC, Bouirden L. Enthalpies of formation of the Al–Nb intermetallic compounds. J Alloys Compd. 1998 Mar;268(1–2):118–121. doi: 10.1016/S0925-8388(97)00554-9
[50] George P, Parida S, Reddy RG. Thermodynamic studies on the system Nb-Al. Metall Mater Trans B. 2007 Feb;38(1):85–91. doi: 10.1007/s11663-006-9011-4
[51] Boer F. Cohesion in metals: transition metal alloys. 1988. North-Holland. Cohesion and structure.
[52] Colinet C, Pasturel A, Nguyen Manh D, et al. Phase-stability study of the Al-Nb system. Phys Rev B. 1997 Jul;56(2):552–565. doi: 10.1103/PhysRevB.56.552
[53] Quist W, Wekken C, Taggart R, et al. Intermediate compound Ni_8Nb in nickel-rich nickel-niobium alloys. Trans Met Soc AIME. 1969;245(2):345–349.
[54] van der Wekken CJ, Taggart R, Polonis DH. Short-range order and the nucleation of long-range order in Ni-rich nickel-niobium alloys. Met Sci J. 1971 Jan;5(1):219–223. doi: 10.1179/030634571790439487
[55] van der Wekken CJ, Larson JM, Taggart R, et al. Analysisof triple dislocations in ordered phases of the type Ni_8X. J Appl Phys. 1972 Nov;43(11):4522–4531. doi: 10.1063/1.1660956
[56] Chen H, Du Y, Xu H, et al. Experimental investigation of the Nb-Ni phase diagram. J Mater Sci. 2005 Sep;40(22):6019–6022. doi: 10.1007/s10853-005-4553-4
[57] Okamoto H. Nb-Ni (niobium-nickel). J Phase Equilib. 1998 Jun;19(3):289–289. doi: 10.1361/105497198770342508
[58] Tokunaga T, Matsumoto S, Ohtani H, et al. Thermodynamic analysis of the phase equilibria in the Nb-Ni-Zr system. Mater Trans. 2007;48(9):2263–2271. doi: 10.2320/matertrans.MB200713
[59] Ruhl R, Giessen B, Cohen M, et al. Metastable hexagonal close-packed phases in Ni-rich Ni-Nb and Ni-Ta alloys. J Less-Common Met. 1967;13(6):611–618. doi: 10.1016/0022-5088(67)90106-3
[60] Matsumoto S, Tokunaga T, Ohtani H, et al. Thermodynamic analysis of the phase equilibria of the Nb–Ni–Ti system. Mater Trans. 2005;46(12):2920–2930. doi: 10.2320/matertrans.46.2920
[61] Bhedwar HC, Heckel RW, Laughlin DE. The oxidation behavior of aluminide-coated γ'/δ directional eutectics. Metall Trans A. 1980 Aug;11(8):1303–1314. doi: 10.1007/BF02653484

[62] Shoemaker CB, Shoemaker DP. The crystal structure of themphase, Nb-Ni-Al. Acta Crystallogr. 1967 Aug;23 (2):231–238. doi: 10.1107/S0365110X6700252X
[63] Benjamin J, Giessen B, Grant N. Intermediate phases in the ternary system Nb(Cr)-Ni-Al at 1140 deg C. Trans Met Soc AIME. 1966;236:224–226.
[64] Hunt CR, Raman A. Alloy chemistry of $\sigma(\beta U)$-related phases: I. extension of μ- and occurrence of μ'-phases in the ternary systems Nb(Ta)-X-Al (X=Fe, Co, Ni, Cu, Cr, Mo)*). Int J Mater Res. 1968 Sep;59 (9):701–707. doi: 10.1515/ijmr-1968-590903
[65] Paulson NH, Bocklund BJ, Otis RA, et al. Quantified uncertainty in thermodynamic modeling for materials design. Acta Mater. 2019;174:9–15. doi: 10.1016/j.actamat.2019.05.017
[66] Zhu LF, Grabowski B, Neugebauer J. Efficient approach to compute melting properties fully from ab initio with application to Cu. Phys Rev B. 2017 Dec;96(22):224202. doi: 10.1103/PhysRevB.96.224202